NASA CR-598

ATTITUDE DETERMINATION BY KALMAN FILTERING

VOLUME I

By James L. Farrell

Prepared under Contract No. NAS 5-9195 by
WESTINGHOUSE ELECTRIC CORPORATION
Baltimore, Md.

for Goddard Space Flight Center

NATIONAL AERONAUTICS AND SPACE ADMINISTRATION

For sale by the Clearinghouse for Federal Scientific and Technical Information
Springfield, Virginia 22151 – Price $2.50

ABSTRACT

To improve the reliability of satellite attitude determination systems, it is desirable to replace complex instrumentation by crude measuring devices with sophisticated data processing. A minimum variance scheme using magnetic and solar measurements is evaluated in a unified simulation applicable to spinning and nonspinning earth or sun orbiters. The simulation program obtains linearized ensemble statistics of the rotational uncertainties, and also generates a Monte Carlo sample which contains the effects of dynamic and geometric nonlinearities.

The Monte Carlo sample is a reasonable member of the linearized statistical population, provided that certain favorable conditions are maintained. Specifically, the above-mentioned sources of nonlinearity must be minimized through the use of an appropriate dynamical formulation and through methodical restriction of measurement geometry.

In connection with rotational dynamics it is noted that spinning orbiters are naturally associated with an inertial reference, whereas gravity gradient satellites are more readily compared with a local frame. The present unified formulation would presumably be sacrificed in actual operation, then, and the inertial formulation employed herein would be maintained only for spinning vehicles. The accuracy of locally linearized gravity gradient libration equations, used thus far only for verifying numerical integration, supports the concept of a local reference with minimum variance attitude determination for nonspinning satellites.

Measurement geometry requirements involve the use of adequate reference lines and the allowable values of measured quantities. A single observable reference line is insufficient for a complete definition of orientation whereas two, preferably orthogonal, lines in space can provide a useful reference for linearized attitude determination. Angular measurements between nearly colinear axes must be avoided, since the algebraic sign of the observed deviation from nominal measurement value is ill-defined. The influence of geometric nonlinearities can be reduced by restricting allowable measurements to large angles.

For spinning satellites the rotational motion is governed primarily by initial conditions, rather than external torques. The orientation and angular rates of the vehicle can therefore be accurately approximated by homogeneous equations with known solutions. By direct differentiation, the transition matrix can be obtained in closed form. This provides a considerable saving in computation, for both the simulation program and any future operational system.

Prior to mechanization of an operational system, all available means of improving the performance should be incorporated. The data conditioning procedures devised herein should be optimized, to maintain maximum attitude information through angular observations while still rejecting all undesirable measurements. Additional observation provisions should be utilized whenever available, and means of compensating nonlinearities should be investigated.

FOREWORD

This work was supported by Goddard Space Flight Center, through NASA Contract No. NAS 5-9195, under the direction of Mr. E.R. Lancaster. The writer gratefully acknowledges this direction and the guidance of the University of Maryland thesis committee: Dr. T.C. G. Wagner (Chairman), Dr. A. Marcovitz, and Dr. R. Hochuli, of the Electrical Engineering Department; and Dr. Peter Musen of the Astronomy Department. Appreciation is also expressed to Mr. Charles Weaver of Westinghouse, for programming all digital computations.

TABLE OF CONTENTS

LIST OF FIGURES

INTRODUCTION

Increasing demands imposed upon both the capability and the durability of space systems have placed reliability at a premium in numerous phases of artificial satellite operation. In connection with attitude determination the desire for reliability is often compromised by the complexity of the associated instrumentation. The question arises, then, as to whether angular information sensing can be limited to crude measurements and whether elaborate instrumentation can be replaced by sophistication in data processing. This possibility has been investigated in detail, and a number of encouraging developments have resulted.

The application of recursive minimum variance smoothing to crude measurements with statistically independent errors has been evaluated using a unified computer program, capable of simulating spinning or nonspinning satellites in orbit around either the sun or the earth. The program obtains linearized ensemble statistics of the rotational uncertainties and, in addition, carries a Monte Carlo sample in which all dynamic and geometric nonlinearities are taken into account. This is done simply by computing the measurement sensitivities, and the dynamical partial derivatives used for time extrapolation of error statistics, from an observed pattern of rotational motion with randomly generated errors carried through an actual nonlinear simulation.

Furthermore, for spinning satellites, the presence of small torques (from solar radiation and, for earth satellites, gravity gradient) was ignored in the computation of the dynamical partial derivatives; they were computed from closed form expressions presented for the first time herein. This computational technique represents a significant saving in mechanization complexity; the procedure can be justified by a brief synopsis of pertinent results:

Under certain favorable measurement conditions, to be described shortly, the Monte Carlo simulation sample provides a reasonable comparison with linearized statistical predictions. In simulation trials with a total initial attitude uncertainty of approximately 0.2 radian, the uncertainty was reduced to 0.02 radian. Angular rate uncertainty was reduced by about the same factor.

The simulation was also applied to the nonspinning case (in particular, an earth satellite locally stabilized by gravity gradient), with somewhat less successful results. The attitude uncertainty was actually reduced by a significant factor, but nonlinear growth of angular rate uncertainty was becoming increasingly apparent as the simulation progressed. For this reason, and for reasons connected with the inherent basic properties of local stabilization, it is believed that the present unified formulation should be sacrificed. The inertial attitude reference utilized here is naturally adapted to spin stabilized satellites. Gravity gradient stabilization, however, is more naturally linearized about a local reference frame.

In regard to measurement requirements it is verified that a single reference line in space is generally inadequate, particularly when an appreciable component of angular rate exists about that line. A pair of observable reference lines, preferably 90 degrees apart, will provide a useful reference. Equally as important, the acceptance of small angle measurements must be discouraged because of geometric nonlinearities. This point can be interpreted from several standpoints (e.g., ill-defined planes, large second derivatives, slope of sinusoidal curves, geometry of intersecting cones). As with all phases of this study, some qualitative comments are offered in subsequent discussion, while detailed mathematical treatment is contained in the Appendix.

The results of this exploratory study indicate the conditions for feasibility of attitude determination with crude instruments by recursive minimum variance data processing. Operational systems will require refinements such as additional observables and/or compensation of recognizable nonlinear effects. These conclusions evolve from the subsequent material in which the basic problem is described, followed by a gradual emergence of the complete model for solution, and finally the outcome of the study and its implications upon physical system mechanization and performance.

STATEMENT OF THE PROBLEM

Methods of Attitude Determination

Existing techniques for establishing an angular orientation commonly employ one of the following means of instrumentation:

1. A gimbaled inertially stabilized or Schuler tuned platform.[1] Used for inertial navigation in applications where mechanical complexity is not prohibitive. Typical drift rate: less than 0.1 degree per hour.

2. A strapdown "analytic platform" in which the above mentioned gimbal configuration is replaced by a high-speed electronic computer unit.[2-6] The remainder of the system is similar to a gimbaled platform, but the dynamical environment of the instruments is naturally more severe.[7, 8] Expected typical drift rate: 0.1 degree per hour.

3. A star tracker, or a combination thereof.[9] Theoretical accuracy: less than 1 second of arc.

4. Star field measurements[10] for correlation mapping. Typical accuracy: 0.1 degree.

5. Horizon scanning devices.[11] Typical accuracy: on the order of 0.5 degree.

6. Geomagnetic and/or solar data.[12, 13] Typical accuracy: 1 to 2 degrees.

7. RF techniques: Interferometer; 0.1 degree typical accuracy. Conical scan or polarization measurements; 1 degree typical accuracy.[14]

Additional techniques not included above utilize instruments which are sensitive to translation as well as rotations (e.g., bubble levels) and other devices (such as ion sensors, TV cameras, or radar sensors) which apparently show some promise for applications in the near future.

Many of the instrumenting techniques itemized above carry an implicit requirement for sophisticated mechanization (e.g., items 1 - 4) and/or restriction to near-planet operation with additional yaw sensing (item 5). An effort to reduce the complexity of the monitoring scheme is evident from item 6, in which simultaneous observations are grouped to form instantaneous attitude fixes from simple measuring devices. Item 7 illustrates a procedure whereby the attitude of a space vehicle is determined by ground based measurements.

These latter examples suggest the desirability of investigating techniques for attitude determination, in which the onboard instrumentation requirements can be relaxed through elaborate communication or data processing. The usefulness of such a scheme is further evidenced by a problem statement recently submitted to SIAM REVIEW[15] and by NASA sponsorship of a 1-year study contract (Contract No. NAS 5-9195; Goddard Space Flight Center) to establish feasibility of an approach utilizing smoothed data taken from simple sensing devices.

Attention will now be directed toward the basic principles and implications of this scheme.

Simplified Measuring Scheme

In an effort to use simplified measuring devices to find the attitude of a space vehicle, it is instructive to consider a straightforward approach described as follows: Characterize the unknown attitude in terms of certain parameters. Express the measured quantities in terms of these parameters. Devise a measurement schedule in which the number of independent observations is chosen equal to the number of rotation parameters. The prescribed series of measurements will then provide a set of equations with an equal number of unknowns. A method of solving these equations would then be sought, in order to yield the desired angular information.

The approach to attitude determination is complicated by all of the following factors:

1. In general the rotation parameters will have unequal deviations from their observed or estimated values.

2. The rotation parameters will not usually be directly measurable; the observed quantities will be dependent upon these parameters through some mathematical (almost certainly nonlinear) relationship. It will thus be necessary to find the appropriate inversion. However, for a system of nonlinear equations, the solution will not be unique. Furthermore, even with the uniqueness problem solved, the inversion

of a set of simultaneous nonlinear equations could be difficult to mechanize. While approximations in the measurement functional relationships could simplify the mechanization, the errors thus incurred would be subject to further analysis and justification.

3. It will not normally be immediately apparent how to choose, from a limited field of available measurements, those observations which will provide the most favorable combination of attitude information. An arbitrarily selected group of simple observations, however, may be ill-conditioned (i. e., the sensitivities of measurements to the rotation parameters may have an undesirable distribution). In an extreme case this could destroy the independence of the chosen measurement set, or one rotation parameter might be unrelated to every measured quantity. Poor conditioning of input data will transform small input errors (due to roundoff in computation and inexact measurements) into unduly large errors in the attitude estimate.

4. The measurements cannot be expected to have equal accuracies and, with an uncontrolled distribution of measurement sensitivities, equally accurate measurements would still not be equally informative. It follows that uniform weighting of incoming data is not an optimum procedure.

5. Rotational dynamics will influence the attitude estimation error as well as the attitude itself. In order to take advantage of all available information, then, an attitude determination system should contain provisions which would account for dynamic propagation

characteristics. This would allow both the extrapolation of previous data and the increased flexibility of using nonsimultaneous measurements.

6. Rotational dynamics are introduced into the system through Euler's equations. Since the equations of motion contain angular acceleration, their solution must include angular rates as well as orientation. The group of rotation parameters to be determined will thus be extended in this application. It is desired that this be accomplished without incurring the additional requirement of angular rate sensing.

7. Repeated observations should be used to offset the upward trend which naturally accompanies an unattended propagation of error with time. This offsetting is most effectively accomplished by choosing measurements on the basis of highest sensitivity to those rotation parameters with the largest instantaneous statistical estimation error.

8. To derive maximum benefit from repeated observations, incoming data should be used to augment, rather than replace, previous information. A weighted average of past and present data will offer the possibility of obtaining an attitude estimate with better accuracy than that of the measurements themselves. The degree of success in this effort will depend upon the autocorrelation time of the measurement error, the rapidity of processing incoming data, and the rate of error propagation due to rotational dynamics.

From the above discussion it is seen that the attitude determination problem is closely paralleled by orbital navigation. The navigation scheme uses the propagation characteristics of errors predicted from Newton's laws in a known force environment. A complete satellite attitude determination system would extrapolate errors using rotational state transition properties obtained from Euler's equations in a known torque environment.* It follows that this is a natural assignment for the Kalman filter,[17,18] of which the celestial applications have thus far been slanted heavily toward navigation for translational position (see, for example, references 19-21).

The main objective of this investigation, then, is to establish the feasibility of attitude determination by recursive minimum variance data processing. The scope of the investigation will be dictated by the following guidelines:

* The analogy of course is by no means perfect. Force-free translational motion is described by a simple straight line, whereas force-free rotation can take the form of combined spin and posigrade or retrograde precession.[16] Translational motion of interest in the navigation problem is governed primarily by a large central force, whereas rotations will sometimes (particularly with spin stabilization) depend principally upon initial conditions, with torques acting as small perturbations. Also, as explained in the next section, there is a basic difference between types of singularities encountered in the two problems.

1. The study will be applicable to both spinning and nonspinning satellites, and to both earth and sun orbiters.

2. The torques to be considered are those due to solar pressure and, for earth orbiters, gravity gradient.

3. Available measurements consist of independent sunline observations and, for earth orbiters, magnetometer readings. All of these observations pertain to on-board sensors.

4. Discrepancies arising from approximations in mechanized functional relationships, and the possible dependence of these discrepancies upon the rotational motion pattern, will be included in the investigation.

5. Included also in this development will be an investigation of available observations which offer the greatest potential reduction in estimation error[21] and avoiding measurements which introduce errors through the mechanized analytical model.[22]

The specific method of achieving the study objective, consistent with all of the above guidelines, will now be described in detail.

FORMULATION OF THE PROBLEM SOLUTION

The largest single factor contributing to the acquisition of quantitative results is the development of a double precision FORTRAN IV digital computer program. This effort, however, must obviously be supported by adequate background analysis, verification, and system considerations which will provide maximum insight into the operation. These functions are discussed separately below, followed by a description of the digital simulation program.

Analytical Approach

Since the program envisioned here involves an extensive range of subject matter, it is desirable to adopt any simplification which will not affect the attitude determination system performance. In this investigation, for example, it makes no difference whether an onboard data processor is used or a communication link is established for earth reduction of attitude measurement data. Also, since the attitude determination system is not critically dependent upon the exact nature of accompanying translational motion, both the deviations of the vehicle orbit from Keplerian motion (due to orbital perturbations) and the small uncertainties in translational position (due to imperfect tracking and navigation) can be ignored. In general, astronomical geometry and dynamics are idealized without hesitation wherever permissible.

The above points facilitate answering the inevitable questions: To what coordinate frame is the vehicle attitude referenced? Also, are the vehicle angular velocities defined with respect to any particular standard?

A partial answer to these questions can be inferred from the angular rate terms in Euler's equations of motion. Although these are resolved into vehicle axes, physically they represent absolute rates (i.e., with respect to an orthogonal triad having an inertially fixed orientation). It is therefore appropriate to utilize the concept of an inertial attitude reference; this can readily be done by adopting the standard celestial sphere model.[23] In keeping with the previously mentioned astronomical idealizations the reference radii of the celestial sphere will have inertially fixed directions, and there is a simple standard transformation[24] between these axes and the vehicle location. This latter transformation will provide a tangible means of expressing vehicle attitude with respect to the orbital pole and the instantaneous local vertical (see Appendix A).

Given the above concepts, there remains the choice of a parameter set for expressing the space vehicle orientation. Although the attitude could conceivably be expressed by a variety of formulations,[25] most of these contain inherent redundancies. In the problem under consideration, redundancy is undesirable since the Kalman filter operates in conjunction with a state vector defined here as follows: Complete solution of Euler's equations in a known torque environment requires a knowledge of six "constants" of integration (these "constants" actually depend upon

the reference time with which they are associated; they are referred to hereafter as state variables). A state vector is a 6 x 1 matrix of state variables, constituting an independent set of parameters capable of defining a unique motion pattern. In this application the state vector consists of three orientation parameters* (e.g., three Euler angle rotations with a specified convention) and three angular derivatives (e.g., roll, pitch, and yaw rate). After the choice of conventions to be used, Euler's equations of motion (which express the vehicle rates and their derivatives in terms of applied torques as shown in Appendix B) and Euler's geometric equations (which relate the Euler angles and their derivatives to the vehicle rates as shown in Appendix C) can be written in state variable form. These expressions constitute a basis for the dynamics of rotational state vector deviations (from a reference angular trajectory) and uncertainties (i.e., estimation errors), as well as the

* In contrast to the translational navigation problem (in which the presence or absence of singularities will depend upon the generalized coordinates used), it is impossible to have an all-attitude three-parameter set without singular points for the rotation group.[25] This significantly influences the conventions adopted for attitude representation and, consequently, the physical system mechanization. The coordinate axes to which the vehicle attitude is referenced are repeatedly shifted, to avoid singularity.

rotational behavior of the space vehicle itself. In combination with the geometry relating the instantaneous state to the observations, a complete analytical model is thus formed which lends itself readily to direct application of the Kalman filter formulation.

Verification

Many of the computations performed in the simulation lend themselves to extremely simple interpretation and verification. In the areas of rotational dynamics, however, there is a significant amount of detailed analysis followed by numerical integration. While verification through direct computation would thus be time-consuming there are, fortunately, certain closed form expressions which adequately describe various aspects of the dynamics for cases of practical interest, enumerated as follows:

1. Spin stabilization of a satellite is associated with the condition of dynamic symmetry about one axis. There is a well-known closed form solution for the rotation of such a satellite in a torque-free environment; both the angular rate vector and the attitude can be expressed directly in terms of the initial conditions. This is thoroughly described in Appendix D.

2. Recent studies of spinning satellites have shown that the small torques produced by gravity gradient[26] and solar radiation[27] can be taken into account in a straightforward manner. This is discussed in Appendix E.

3. A nonspinning case of considerable interest is the satellite which is locally stabilized by gravity gradient. Appendix F contains a detailed libration analysis for a satellite with an arbitrary inertia ellipsoid.[28] (Although these results are correct for "sufficiently small" angular displacements in the general case of three arbitrary principal moments of inertia, they are subject to certain unexpectedly severe restrictions;[29] these are of course observed in choosing simulation trials.)

Each of these checks is made in every applicable simulation trial; this is done simply by programming the additional computation, logic, and readout instructions. The numerical integration control is then set such that all significant digits of all attitude matrix elements agree with the corresponding closed form solution for the symmetrical torque-free satellite. A four-digit agreement is then obtained for spinning satellites with nonzero torque, under typical simulation conditions. The gravity gradient libration computations, although understandably less accurate, provide a useful check for approximate vehicle attitude (i.e., accurate to within a few percent).

Although the simulated equations of motion are in no way dependent upon these check solutions, further benefits were drawn from the closed form expressions at a later point in the program. The linearized extrapolation of estimation error statistics, between measurements in the Kalman filter, requires a matrix of dynamical partial derivatives. In this application the matrix consists of the first order sensitivities of

vehicle rates and orientation parameters with respect to the initial conditions. While this causes no problem in connection with slowly rotating (e.g., gravity gradient stabilized) satellites, it was found that the numerical integration of these sensitivities consumed excessive amounts of machine time for spinning vehicles. The difficulty was sidestepped completely through derivation of another set of closed form expressions as follows: The state variable equations of motion shown in Appendix G were rewritten for the homogeneous (zero torque) case. This is an accurate representation of spinning satellite motion, for any reasonable time interval between measurements. Since closed form equations of motion are available in the homogeneous case, the dynamical partial derivatives can be obtained directly by differentiation. * The complete analysis is presented in Appendix H; at this point it is worth noting that (1) a closed form rotational state transition matrix has not appeared previously in the literature (although an alternative formulation for a similar attitude determination system using star trackers is being studied by Dr. S. F. Schmidt of the Philco Corporation), and (2) it has been verified by simulation that, under torque-free conditions, the closed form matrix is in agreement with the corresponding matrix obtained by numerical integration.

* This is somewhat analogous to the procedure described in Reference 22, in which a Keplerian transition matrix was used for navigation. The writer is indebted to Dr. Samuel Pines for suggesting this technique.

System Concepts

Because of the well-known linear transformation properties of gaussian random processes, the use of Kalman filtering in linear systems with white noise ensures predictability of statistical behavior of the estimation error at all times. The simulation of a system which is not perfectly linear, however, can betray the presence of estimation errors beyond the level predicted by linearized analysis. It is of interest at this point to consider the reasons for this phenomenon, and to indicate briefly the implications upon system mechanization.

For maximum insight into the problem, this discussion will begin with a simplified functional representation of the procedures used for data processing. Consider first the hypothetical case of a single observable line (e.g., the sightline to the sun) having known direction cosines (l_1, m_1, n_1) with respect to a specified coordinate frame. Assume that an angle (a_1) can be measured between this observable line and any vehicle reference line (e.g., the roll axis of a satellite) having an unknown orientation with respect to the reference coordinate frame. In principle, an equation could be written involving the unknown direction cosines (l, m, n) of the roll axis, i.e., $l_1 l + m_1 m + n_1 n = \cos a_1$. In addition, the sum of the squares of the unknowns must be unity by definition. The absence of a third relation, however, precludes a complete determination of the roll axis orientation. Physically the measurement of the angle (a_1) places the roll axis on a cone of revolution about

the sunline, but does not specify the particular element of that cone to be identified with the roll axis. The problem generalizes immediately to a complete attitude determination for satellite roll, pitch, and yaw axes; a single observable reference line can provide satellite attitude information only to within an unknown angle of rotation about that line. When the example is extended further to account for satellite rotational motion, the difficulty is obviously increased; this is particularly true when there is a large component of angular velocity about a line instantaneously parallel to the observable reference.

The problem of attitude uncertainty propagation with a single observable reference line can now be clarified. The time extrapolation of error statistics between measurements, mechanized in the minimum variance data processor, is obtained by a truncated (first order) Taylor series expansion. The actual behavior of the error statistics may remain close to the mechanized relation for a limited time but, as the process continues with a permanent deficiency in attitude information, significant departures will occur. At the same time, the Kalman filter weighting coefficients will be computed from the linearly extrapolated estimation error statistics, as illustrated in Appendix I. The filter equations will then predict, as a result of each measurement, an estimation error reduction which in reality never occurred. It follows immediately that an estimate computed from linearized weighting coefficients can contain errors beyond the predicted statistical level.

The situation depicted above is markedly improved by introducing a second observable reference line. While conceivably this paves the way for a host of geometric and mathematical interpretations, it suffices here to note the following items:

1. The optimum separation of the two observable reference lines is a right angle.

2. Exact determination of orientation for a given satellite axis, by the method under present consideration, is tantamount to locating a unique element which is common to two tangent cones.

3. The presence of errors in the system could introduce ambiguities (in the case of doubly intersecting cones) or inconsistencies (in the case of nonintersecting cones) if attitudes were determined explicitly from simultaneous measurements. In the Kalman filtering scheme these effects would appear as sources of nonlinearity.

4. The effects noted above are most severe when the vehicle axis under scrutiny is instantaneously in the plane of the two observable reference lines. The reason is simply that small errors could easily prevent the cones from intersecting under these conditions or, if the cones do cross, the two lines of intersection are too close to allow resolution of the correct orientation.

5. The difficulties noted above can be minimized by restricting the allowable measurements to large angles.

This last item is closely associated with the concept of mechanized selection of observations, introduced in an earlier discussion of study

guidelines. The pertinent mathematical derivations, as applied to sun-line and earth magnetic field measurements, appear in Appendices J and K, respectively. These last two appendices complete the entire mathematical formulation for the study. The complete analysis is combined into a double precision digital simulation, described below.

Program Configuration

The block diagram for a Kalman filtering system simulation with scalar measurements* appears in figure 1. The measurement data points (y), as always, are obtained by comparing an observation (Y) with its predicted value ($Y^{(-)}$). These observable values, in turn, are determined with the aid of the (in general, nonlinear) transformations $H\left\{\Phi\left(\underline{X}_o\right)\right\}$ and $\hat{H}\left\{\hat{\Phi}\left(\underline{\hat{X}}_o\right)\right\}$, respectively, where H and Φ denote geometric and dynamic transformations, respectively, and a circumflex denotes observed quantities in all cases. While the weighting of the data points $\left\{\underline{W}_{\underline{y}}^{\wedge}\right\}$ and the uncertainty covariance matrix extrapolation (not shown on figure 1) are necessarily linear, it should be noted that actual nonlinear transformations are utilized wherever applicable and the simulated data processor has access only to observed parameters throughout. The model thus accounts for all errors incurred through dynamic and geometric nonlinearities.

---

* This includes the case of simultaneous but statistically independent measurements.

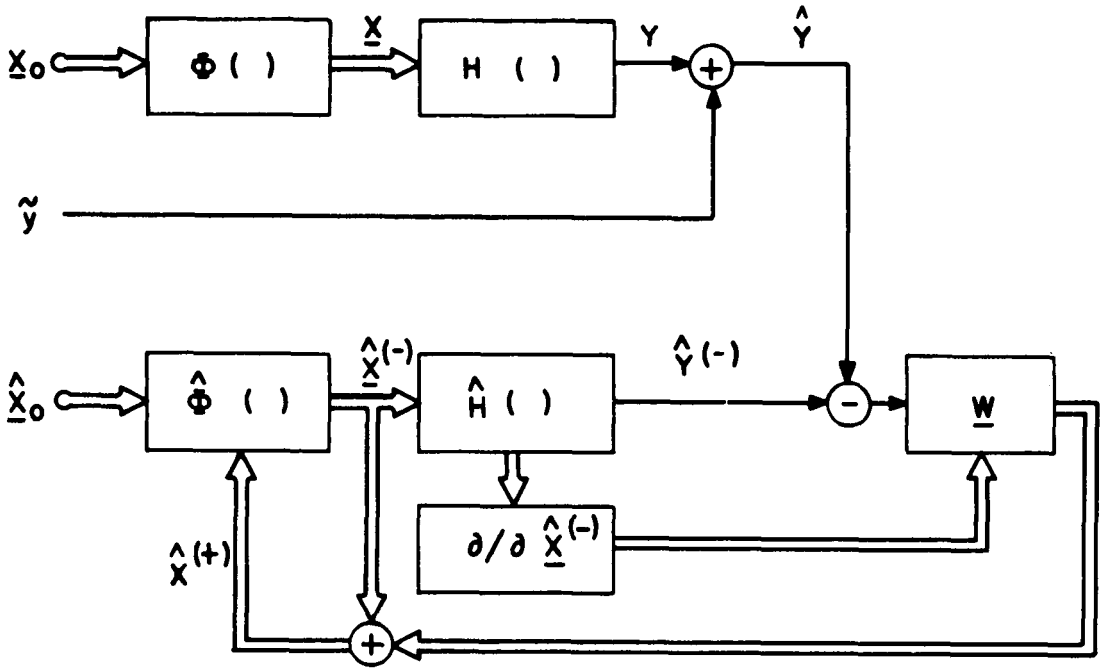

Figure 1. Simulation Block Diagram

RESULTS AND INTERPRETATIONS

Simulation Trial Conditions

From the innumerable combinations of conditions which the program can simulate, the following inputs were chosen for data acquisition and presentation:

- Orbital geometry. - Solar orbiters were placed in circular paths in the ecliptic, at one astronomical unit from the sun. Earth satellites were placed in equatorial circular orbits of low altitude.

- Vehicle configuration. - Spinning satellites were given moments of inertia of 150, 100, and 100 kg-meter^2 about the roll, pitch, and yaw axes, respectively. The same values were used for locally stabilized satellites, except for the pitch axis value (200 kg-meter^2). For earth satellites, the center of gravity was made coincident with the center of pressure, whereas a 1-meter separation along the symmetry axis was adopted for sun orbiters. Effective vehicle area was set at 100 meter^2.

- Observation parameters. - Sun orbiters were given a total of twelve sun sensors (Appendix J) with rms accuracies of 0.01 radian. This provided each vehicle sighting reference (+roll; -roll; +pitch; etc.) with two 64° field-of-view sensor faces; each sun sensor pair was arranged to have a slit separation of 90 degrees. Earth satellites were given the same array of sun sensors, plus three magnetometers

with rms accuracies of 10^{-6} weber/meter^2. Measurement intervals were 1 second and 30 seconds for spinning and locally stabilized satellites, respectively.

- Initial conditions. - Sun orbiters were set spinning with 1 radian per second angular rate about the symmetry axis and one percent intrinsic precession. The spin axis was placed at various angles with respect to the sun for various trials, in order to illustrate the effect of this angle upon performance. For earth orbiters, both the sun and the magnetic pole were placed at zero longitude* on the appropriate celestial sphere (Appendix A). Spinning earth satellites were given angular rates of 1 radian per second about the symmetry axis, and 5 percent intrinsic precession; the spin axis was inclined at 30 degrees with respect to the sun. Gravity-gradient stabilized satellites were given roll, pitch, and yaw peak displacements of 0.05, 0.03, and 0.04 radian, respectively, off the local reference.

Initial rms uncertainties were set at 0.1 radian and 0.05 radian per second for angular displacement and angular rate in each axis, respectively, for spinning satellites. A similar procedure was followed for locally stabilized satellites, but with angular rate uncertainty changed to 10^{-4} radian per second in each axis.

* In combination with other program inputs, the initial placement of these vectors provided an initial angular displacement of approximately 79 degrees between the sunline and the magnetic flux density vector.

• Data processor configuration. - For spinning satellites the transition matrix was computed in closed form, by ignoring the small torques. For the locally stabilized case, dynamical partial derivatives were integrated numerically from the nonhomogeneous equations of rotational motion.

Data Presentation and Discussion

The above standard conditions were applied to the following simulation trials:

• Case 1 A. - A spinning solar orbiter was simulated with the symmetry axis essentially normal to the orbital plane. Sun sensor observations were restricted to accept only those measurements for which (a) the instantaneous angle (ζ) between the sensor slit and the sunline exceeded $\pi/4$ radian, and (b) the measured angle (i.e., the angle between the slit-sunline plane and the sensor face) was between $\pi/4$ and $3\pi/4$ radians.

• Case 1 B. - The above run was repeated for a 60 degree inclination between the spin axis and the sunline.

• Case 1 C. - Inclination of the spin axis with respect to the sunline was changed to 30 degrees.

• Case 2 A. - A spinning earth satellite was simulated under conditions defined above with a 30-degree inclination between spin axis and sunline. Magnetometer observations were restricted, to exclude field

measurements along any line within $(\pi/2 - 0.2)$ radians of the flux density vector.

- Case 2 B. - The preceding trial was repeated, but with essentially unrestricted acceptance of all solar observations within the instrument field of view.

- Case 2 C. - All magnetometers were deactivated, under conditions otherwise equivalent to case 2 A.

- Case 3 A. - An earth satellite, locally stabilized by gravity gradient, was simulated with the following measurement restrictions: (a) the minimum acceptable angle (ζ), defining the slit-sunline plane (see the preceding discussion of case 1 A), was 1 radian; (b) the same restrictions as those used in cases 1 A and 2 A were adopted for the measured angles and magnetic field components, respectively.

The results of cases 1 A, 1 B, 2 A, 2 B, and 3 A are plotted in figure 2. The figure shows both the ensemble statistics (computed from linearized covariance matrix equations) and a Monte Carlo sample which was simultaneously carried through the actual nonlinear equations. *

* The Monte Carlo sample attitude error is defined rigorously as the square root of the sum of the squares of the positive off-diagonal terms of the error matrix. The error matrix is the apparent transformation from vehicle to inertial coordinates, premultiplied by the inverse of the actual direction cosine transformation from true vehicle axes to the same inertial reference. This is computed at the end of each measurement interval.

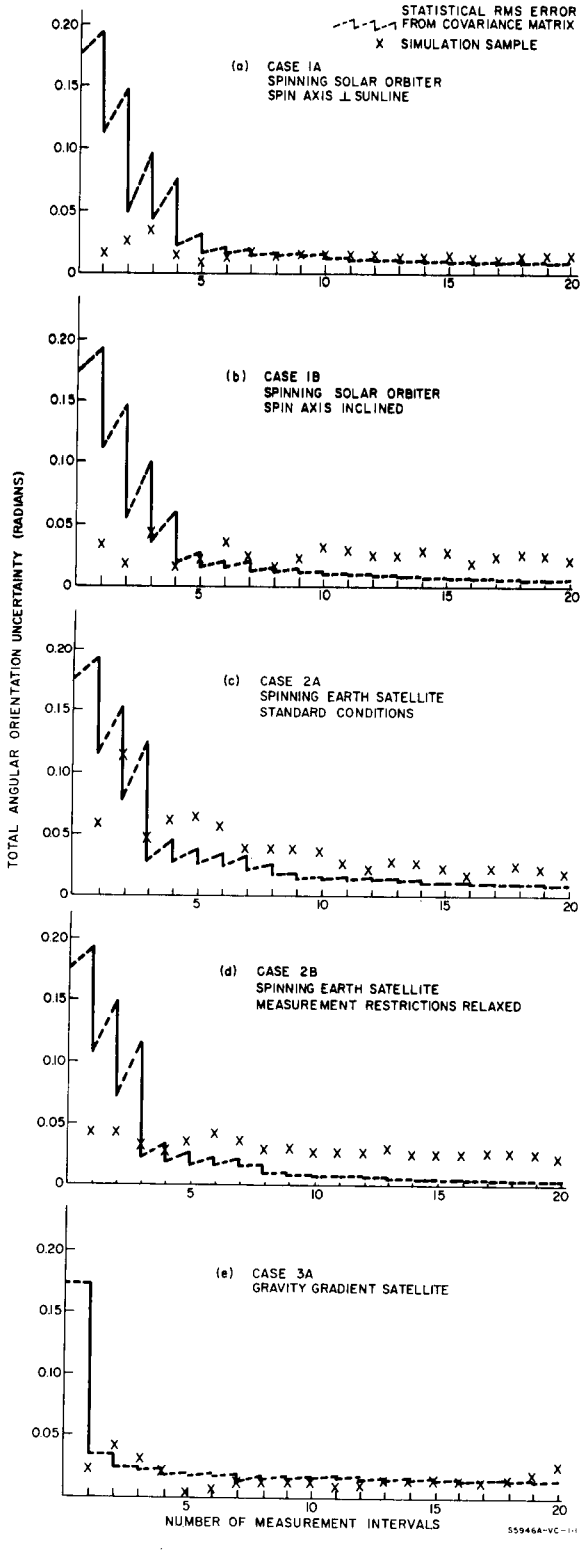

Figure 2. Total Attitude Uncertainty vs Time

The rms total error is the square root of the trace of the corresponding uncertainty covariance matrix. These graphical results are supplemented by the following additional data:

1. At the end of case 1 A, the Monte Carlo sample angular rate uncertainty was well within the 1-sigma level of the linearized prediction. At the end of case 1 B, however, the angular rate uncertainty was beyond 3-sigma.

2. In case 1 C, the angular orientation error of the Monte Carlo sample was temporarily reduced after a few measurements, but quickly grew to more than 10-sigma.

3. Although the sample resultant angular rate uncertainties in cases 2 A and 2 B did not exceed 3 sigma, both cases contained uncertainties near the 3-sigma level for individual components of the angular rate vector.

4. The results of case 2 C were comparable to those of case 1 C.

5. At the end of case 3 A, the total angular rate uncertainty of the Monte Carlo sample was beyond 3 sigma; the pitch rate uncertainty, in particular, was near 10 sigma.

Explanations for these results largely follow from previously discussed concepts. Comparison of case 1 A with 1 B and 1 C shows the nonlinear error propagation occurring with angular motion about a single reference line. Comparison of sample behavior relative to linearized statistics in 2 A and 2 B (e.g., in the latter portions of

figures 2c and 2d) illustrates the nonlinearities ultimately introduced by small angle measurements. Case 2 C has the same interpretation as 1 C. In case 3 A, locally stabilized attitude estimates are provided over a short arc (20 intervals separated by 30 seconds corresponds to roughly 1/9 orbit for near-earth satellites).

The sample angular rate uncertainties, mentioned in items 3 and 5 above, deserve added attention here. Whereas nonlinearities were purposely introduced into case 2 B, the sample angular rate uncertainty in 2 A represents an inherent imperfection in the system configuration as mechanized for that trial. Improved performance would be realized by optimizing the allowable range of magnetic and solar measurements through a parametric study. In regard to the gravity gradient satellite, a likely scheme for improving the linearity would be to redefine the state variables in terms of the local reference, using linearized equations in this local coordinate system (of the type shown in Appendix F) to compute dynamical partial derivatives. Relative superiority of certain coordinate systems has been studied in connection with the navigation problem,[30] but similar results have not yet appeared for rotational motion analysis.

The above numerical results serve to illustrate both the capabilities and the limitations of the linearized attitude determination scheme as mechanized in the simulation. Presumably, a more favorable set of input conditions could have been assumed or, conversely, poorer performance could have been exhibited under less favorable

circumstances. The purpose of the data presentation, however, was to illustrate certain effects without being unduly optimistic or pessimistic about the mechanized configuration. In the proper perspective, the results indicate that linearized attitude determination is promising, but increased sophistication would be in order for a complete operational system. Methods for extending the system capability are discussed in the next section.

CONCLUSIONS AND RECOMMENDATIONS

This study has derived the conditions for feasibility of satellite attitude determination by crude instruments, to be used in conjunction with recursive minimum variance data processing. With spinning satellites, the dynamical partial derivatives used for time extrapolation of error statistics can be computed from homogeneous equations in closed form. For nonspinning satellites these partial derivatives should be computed from a local reference. Attitude accuracy obtained using a single observable reference line (e.g., the sunline) is generally much poorer than that obtained with two (e.g., the sunline and the earth magnetic field vector). Optimum separation of the reference line pair is a right angle. Nonlinear effects introduced through incoming data can be controlled by restricting the allowable measurement geometry.

The measurement restriction technique, however, has the additional effect of depriving the system of some attitude information. If carried to extremes, of course, this could transform a double-line reference in space into an effective single reference line system. It is therefore necessary to form an undesirable compromise when only two reference lines are available. It follows that the mechanization of an actual operational system would call for a degree of sophistication beyond that of the configuration assumed for this exploratory study.

One possible improvement for near-earth satellites would be the introduction of additional reference lines, through one-way RF transmission from existing tracking stations. On-board RF sensing methods could be basically similar to present approaches[14] but, since the Kalman filter can accept a variety of information, only a crude and perhaps incomplete array of receiving equipment would be needed. Another improvement in capability would be realized by incorporating data processor modifications to counteract recognizable nonlinear[31] effects (such as large residuals obtained in data reduction or known sensing nonlinearities). Finally, an operational system would account for systematic errors as well as the uncorrelated measurement noise.

APPENDIX

This section contains the entire mathematical background for all dynamic, geometric, and statistical analyses and transformations employed in this study. Much of the theory is well established by a long history of documentation; some was taken from recent contributions to the open literature; and certain portions (specifically, the closed form rotational state transition matrix) have not appeared previously in the literature.

The first three appendices contain straightforward means of describing general angular motion, and Appendix D gives a well known special case solution to the rotational equations of motion. Appendix E discusses the precession of angular momentum due to solar and gravity gradient torques, as described separately in two recent articles in the applicable literature. Appendix F discusses some recent literature regarding gravity gradient libration, and provides a restrictive closed form solution for vertically oriented satellites. The next two appendices adapt the state variable formulation to rotational systems, in preparation for the Kalman filtering operations described in Appendix I. The last two appendices illustrate the types of measurements under consideration and their allowable ranges of variation.

List of Major Notation*

Symbol	Definition
A_v	Effective vehicle area (meter^2)
$\underline{\underline{A}}$	Matrix of coefficients in differential equation for $\underline{\underline{\Phi}}$
a_{ij}	ij element of $\underline{\underline{A}}$
$\underline{\underline{B}}$	Transformation from vehicle to fixed inertial coordinates
$\underline{B}_n$	nth column of $\underline{\underline{B}}$
$\underline{\underline{C}}$	Transformation from vehicle to local coordinates
c_{ij}	ij element of $\underline{\underline{C}}$
$\underline{\underline{D}}$	Transformation from local to fixed inertial coordinates
$\underline{\underline{G}}$	Transformation from vehicle to temporary inertial coordinates.
$\underline{G}_n$	nth column of $\underline{\underline{G}}$
g_{ij}	ij element of $\underline{\underline{G}}$
$\underline{H}$	1 x 6 row vector of partial derivatives $\partial Y/\partial \underline{X}$
$\underline{\mathcal{H}}$	1 x 3 row vector $\left[H_1\ H_2\ H_3\right]$
$\underline{h}$	Angular momentum vector
$\underline{\underline{I}}_{nn}$	n x n identity matrix
$\underline{I}$	Unit vector along fixed inertial x-axis
$\underline{I}'$	Unit vector along temporary inertial x-axis
$\underline{i}$	Unit vector along vehicle roll axis
I	Moment of inertia (kg - meter^2)
i	Orbital inclination angle

* Units for angles and their derivatives are radians and seconds.

Symbol	Definition
$\underline{J}$	Unit vector along fixed inertial y-axis
$\underline{J}'$	Unit vector along temporary inertial y-axis
$\underline{J}_v$	Unit vector along orbit pole
$\underline{j}$	Unit vector along vehicle pitch axis
$\underline{K}$	Unit vector along fixed inertial z-axis
$\underline{K}'$	Unit vector along temporary inertial z-axis
$\underline{K}_v$	Unit vector along upward local vertical
$\underline{k}$	Unit vector along vehicle yaw axis
$\underline{K}_\beta$	Unit vector pointing to north magnetic pole of earth (fixed inertial coordinates)
$\underline{L}_1$	Unit vector normal to face of sun sensor in vehicle (vehicle coordinates)
$\underline{L}$	$\underline{U} \times \underline{L}_1$ (vehicle coordinates)
$\underline{m}$	Earth dipole moment (amp-meter^2; fixed inertial coordinates)
$\underline{N}$	Sensitivity vector in the plane of $\underline{L}$ and $\underline{U}$ (vehicle coordinates)
n_0	Orbital rate
$\underline{\underline{O}}_{mn}$	m x n null matrix (subscripts omitted for m = n = 1)
P_ρ	Solar pressure (Newtons per meter^2)
$\underline{\underline{P}}$	Uncertainty covariance matrix
$\underline{Q}$	Vector from center of pressure to center of gravity in vehicle (meters; vehicle coordinates)
q	Magnitude of $\underline{Q}$
q_n	nth component of $\underline{Q}$

Symbol	Definition
$\underline{R}$	Vehicle position vector with reference to central force field (meters; fixed inertial coordinates)
r	Magnitude of $\underline{R}$
r_1, r_2	Coupled yaw-roll libration frequencies
$\underline{S}$	Unit vector toward sunline (fixed inertial coordinates)
$\underline{S}'$	Unit vector toward sunline (temporary inertial coordinates)
$\underline{S}''$	Unit vector toward sunline (vehicle coordinates)
t	time
$\underline{U}$	Unit vector along sun sensor slit (vehicle coordinates)
$\underline{V}$	Unit vector along ($\underline{S}''$ x $\underline{U}$) (Vehicle coordinates)
$\underline{W}$	Recursive optimum linear estimator
X_1, X_2, X_3	Position state variables (Euler angles)
X_4, X_5, X_6	Velocity state variables (roll, pitch, yaw rates)
$\underline{X}$	6 x 1 state vector
$\underline{x}$	Variation of $\underline{X}$ from reference value
Y	Observable
y	Variation of Y from reference value
Z_{ij}	Coupled yaw-roll libration amplitudes
z_n	Initial value of (nth) angular displacement from local reference
α, α_{hv}, α_{kv}	Angles between reference vectors for rotation analysis of symmetrical satellite

Symbol	Definition
$\underline{\beta}$	Earth dipole magnetic flux density (webers/meter^2; fixed inertial coordinates)
$\underline{\beta}'$	Earth dipole magnetic flux density (temporary inertial coordinates)
$\underline{\beta}''$	Earth dipole magnetic flux density (vehicle coordinates)
β_n	nth component of $\underline{\beta}$
$\underline{\underline{\Gamma}}$	Transformation from local to temporary inertial coordinates
$\underline{\Gamma}_n$	nth column of $\underline{\underline{\Gamma}}$
δ	Variation
δ_1, δ_2, δ_3	Roll, pitch, and yaw libration angles
ζ	Angle between $\underline{S}''$ and $\underline{U}$
$\underline{\underline{\eta}}$	Time-varying orientation matrix for torque-free symmetrical satellite
θ	True anomaly
λ	Vehicular elevation angle
μ	Gravitational constant of central force field (meter^3/sec^2)
μ_β	$4\pi \times 10^{-7}$ henry/meter
ν	Dynamic coefficient (/sec^2)
ξ	Dynamic coefficient (dimensionless)
ρ	Force due to solar pressure (Newtons)
σ	Standard deviation (general)
$\underline{\underline{\Phi}}$	State transition matrix

Symbol	Definition
ϕ_{ij}	ij element of $\underline{\underline{\Phi}}$
Ψ_{ij}	Coupled yaw-roll libration phase angles
ψ	Vehicular azimuth angle
Ω	Longitude of ascending node
ω_A, ω_B	Spin and precession rates for torque free symmetrical satellite
ω_n	nth component of vehicle angular rate vector (n = 1, 2, 3)
ω_0	Argument of perigee of vehicle orbit
ω_ρ	Precession rate
ω_s	Sidereal rate
Subscripts	
1, 2, 3	Pertaining to x, y, and z axes, respectively
x, y, z	Pertaining to x, y, and z axes, respectively
m	At time of mth observation
0	Orbital, initial
s	pertaining to sun
β	pertaining to earth magnetic field
$\underline{\ }$	vector
$\underline{\underline{\ }}$	matrix
Superscripts	
$(\hat{\ })$	Observed or apparent value
$(\tilde{\ })$	Error in observed or apparent value
(+)	Immediately after an observation

Symbol	Definition
$(-)$	Immediately before an observation
$( )^T$	Transpose
$( )'$	Pertaining to temporary inertial coordinates
$( )''$	Pertaining to vehicle coordinates
Special Notations	
Υ	Vernal Equinox
$\left[\gamma\right]_u$	Orthogonal transformation matrix corresponding to a positive rotation of (γ) radians about the u-axis.

APPENDIX A

COORDINATE REFERENCES

As explained in the Introduction, the need for an inertial attitude reference has prompted the use of the familiar celestial sphere. For earth satellites the earth is considered as the center of the celestial sphere, but it is permissible to have the sun at the center for solar orbiters.[23] In either case the reference radii have fixed directions in inertial space, since (as previously discussed) the entire analysis can be conducted on the basis of a somewhat idealized astronomical geometry. Specific analytical interpretations of the celestial sphere for earth satellites and solar orbiters are described separately as follows:

- Earth satellites. - Figure 3 illustrates a coordinate frame having an inertially fixed orientation (right hand set defined in terms of the vernal equinox and the north geodetic pole as shown) and a local vertical frame (right hand set defined in terms of the orbit pole and the instantaneous upward local vertical), with the orthogonal transformation $\underline{\underline{D}}$ between these frames defined by the commonly designated angles.[24] Since the solar "orbit" is characterized by zero nodal longitude and an ecliptic inclination angle (i_s), the unit sunline vector in fixed inertial coordinates is

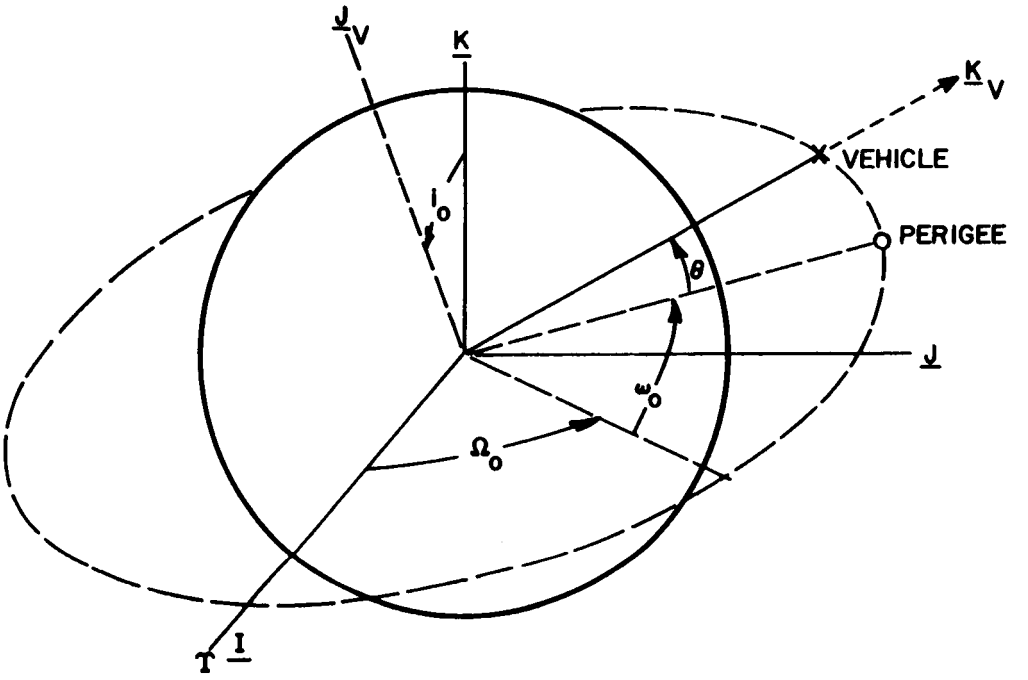

$$\underline{\underline{D}} \triangleq \left[-\Omega_o\right]_Z \left[-i_o\right]_X \left[-(\omega_o + \theta)\right]_Z \begin{bmatrix} 0 & 0 & 1 \\ 1 & 0 & 0 \\ 0 & 1 & 0 \end{bmatrix}$$

SUNLINE

$$\underline{S} = \left[-i_s\right]_X \left[-\theta_s\right]_Z \begin{bmatrix} 1 \\ 0 \\ 0 \end{bmatrix}$$

VEHICLE

$$\begin{bmatrix} \underline{I} \\ \underline{J} \\ \underline{K} \end{bmatrix} = \underline{\underline{D}} \begin{bmatrix} \underline{I}_v \\ \underline{J}_v \\ \underline{K}_v \end{bmatrix}$$

Figure 3. Celestial Sphere

$$\underline{S} = \begin{bmatrix} \cos \theta_s \\ \cos i_s \sin \theta_s \\ \sin i_s \sin \theta_s \end{bmatrix} \tag{A-1}$$

where (θ_s) is determined by the time of the year past March 21.

• Solar orbiters. - With the sun at the center of the celestial sphere, figure 3 is reinterpreted to account for the following modifications:

1. The sunline in vehicle coordinates is along the downward local vertical.

2. The reference line for the true anomaly (θ) is the perihelion.

3. The fixed inertial z-axis is the pole of the ecliptic. The orbital inclination (i_0) is reinterpreted accordingly.

With the above definitions it is now possible to present the remaining attitude formulations, which are uniformly applicable to earth and sun orbiters. If the transformations from vehicle axes to fixed inertial and to local vertical coordinates may be designated as $\underline{\underline{B}}$ and $\underline{\underline{C}}$, respectively, it follows that

$$\underline{\underline{B}} = \underline{\underline{D}}\ \underline{\underline{C}} \tag{A-2}$$

Since the attitude determination procedure involves a formulation in terms of nonredundant parameters (i.e., state variables), we are interested ultimately in a set of Euler angles* rather than the direction cosines themselves. Theoretically there is great flexibility in the choice of Euler angle arrangements and sequences, but the overall

* Although there are other three-parameter sets of attitude variables,[25] there are no all-attitude three-parameter sets without singularities or discontinuities. It follows that Euler angles represent as suitable a parameter set as any other known formulation.

transformation must be defined such that the well-known singularity problem will be avoided. A convenient nonsingular definition of the transformation is derived as follows:

During the "present" interval (i.e., $t_{m-1} < t < t_m$) the true vehicle attitude relative to its true previous (t_{m-1}) orientation is given by

$$\underline{\underline{G}} = \underline{\underline{B}}^T_{m-1} \underline{\underline{B}} \tag{A-3}$$

Combined with equation A-2 and the definition of the known, independently time-varying matrix $\underline{\underline{D}}$ (figure 3), it follows that

$$\underline{\underline{G}} = \underline{\underline{\Gamma}} \underline{\underline{C}} \tag{A-4}$$

where $\underline{\underline{\Gamma}}$ is the time-varying matrix defined in figure 4. It can thus be seen that Euler's equations of motion (which, to look ahead for a moment, contain torques that vary as a function of $\underline{\underline{B}}$ and $\underline{\underline{C}}$) can be written in terms of $\underline{\underline{G}}$ and other transformations which depend only upon the current translational motion and the rotational motion which occurred prior to the interval under consideration. Since these other transformations ($\underline{\underline{B}}_{m-1}$, $\underline{\underline{C}}_{m-1}$, $\underline{\underline{\Gamma}}$) are obviously known during the present interval, the torques in Euler's equations can be considered as known functions of $\underline{\underline{G}}$. This matrix, in turn, can be written as a sequence of roll, pitch, and yaw turns;

$$\underline{\underline{G}} = \left[X_3\right]_z \left[X_2\right]_y \left[X_1\right]_x \tag{A-5}$$

For nonspinning satellites these angles cannot grow to large values (in particular, X_2 cannot grow near $\pi/2$) during any reasonable

AT TIME t_{m-1} , $\underline{\underline{B}}_{m-1} = \underline{\underline{D}}_{m-1}\,\underline{\underline{C}}_{m-1}$

AT TIME t , $\underline{\underline{B}} = \underline{\underline{D}}\,\underline{\underline{C}}$

TRANSFORMATION TO TEMPORARY REFERENCE:

$$\underline{\underline{G}} \triangleq \underline{\underline{B}}^{T}_{m-1}\,\underline{\underline{B}} = \underline{\underline{\Gamma}}\,\underline{\underline{C}};$$

$$\underline{\underline{\Gamma}} \triangleq \underline{\underline{C}}^{T}_{m-1}\,\underline{\underline{D}}^{T}_{m-1}\,\underline{\underline{D}} = \underline{\underline{C}}^{T}_{m-1}\begin{bmatrix}0&1&0\\0&0&1\\1&0&0\end{bmatrix}\begin{bmatrix}\theta_{m-1}-\theta\end{bmatrix}_{Z}\begin{bmatrix}0&0&1\\1&0&0\\0&1&0\end{bmatrix}$$

SUBSTITUTION INTO TORQUE EQUATIONS:

$\underline{\underline{C}} = \underline{\underline{\Gamma}}^{T}\underline{\underline{G}}$	$\underline{\underline{B}} = \underline{\underline{B}}_{m-1}\underline{\underline{G}}$
$c_{ij} = \underline{\Gamma}_{i}^{T}\underline{G}_{j}$	$\underline{Q} \times \underline{\underline{B}}^{T}\underline{S} = \underline{Q} \times \underline{\underline{G}}^{T}\underline{S}'$, $\underline{S}' \triangleq \underline{\underline{B}}^{T}_{m-1}\,\underline{S}$

Figure 4. Shifting Inertial Reference

measurement interval. For spinning satellites, the arbitrary nomenclature of the three vehicle axes can easily be chosen with reference to the initial $\underline{\underline{C}}$ - matrix such that, for a given initial vehicle angular rate and a given dynamical environment, the angle (X_2) could not grow near $\pi/2$ during a specified measurement interval. This convention therefore maintains a well-defined set of Euler angles.

A nonsingular three-parameter set of attitude variables can therefore be obtained by using a temporary inertial reference, which is repeatedly shifted to the orientation corresponding to the time of the most recent measurement. With this formulation, the rotational equations of motion can be written with forcing functions (torques)

which vary as known functions of well-defined Euler angles (X_1, X_2, and X_3). Attention will now be drawn to the form of these forcing functions and the resulting form of the dynamical equations.

APPENDIX B

EULER'S DYNAMIC EQUATIONS

The present investigation is aimed primarily at establishing the feasibility of minimum variance attitude determination, rather than a rigorously precise simulation involving complete characterization of all higher order errors and anomalies. In the interest of obtaining a computer program with a minimum of time-consuming numerical integration routines, the analytical model is idealized to some extent wherever the simplications do not affect the magnitude of the torques to be encountered.

An orbiting satellite with a nonspherical inertial ellipsoid experiences a well known torque due to gravity gradient. It can be shown that, for an ideal inverse square law gravitational field, this torque is*

* Actually it is shown in reference 32 that small gravity gradient torques can be present even when the three principal moments of inertia are equal. Another complication arising from nonideal geometry is the change in torque due to a nonuniform gravity field. Gravity gradient torques with an oblate earth are analyzed in reference 33.

$$\underline{T}_g = (3\mu/r^3) \begin{bmatrix} c_{33}\, c_{32}\, (I_3 - I_2) \\ c_{31}\, c_{33}\, (I_1 - I_3) \\ c_{32}\, c_{31}\, (I_2 - I_1) \end{bmatrix} \qquad \text{(B-1)}$$

As a simple illustration of this expression consider a satellite with z-axis symmetry (so that $I_2 = I_1$) and with $I_3 < I_1$. When the vehicle is nearly aligned with local axes the small angle transformation matrix $\underline{\underline{C}}$ has nearly skew-symmetric off-diagonal elements. If $\underline{k}$ has a positive projection on the $\underline{J}_v$ axis, then (c_{23}) is positive; (c_{32}) is therefore negative, and T_{g1} is positive, essentially proportional to (c_{23}). This tends to align $\underline{k}$ with the local vertical axis $\underline{K}_v$.

In addition to the above torque due to gravity gradient, there is a torque due to solar pressure when the vehicle cg does not coincide with its center of pressure. Assuming specular reflection from a homogeneous spherical surface, the appropriate force (ρ) is the product of the effective vehicle area (A_v) multiplied by solar pressure (9×10^{-6} Newton per square meter at 1.0 AU, and inversely proportional to the square of solar distance).[34] The lever arm is the cross product of the sun-line vector $\underline{S}''$ with the vector $\underline{Q}$ extending from the pressure center to the cg; it follows that the solar torque is

$$\underline{T}_s = \rho\, (\underline{Q} \times \underline{S}'') = \rho\, (\underline{Q} \times \underline{\underline{B}}^T\, \underline{S}) \qquad \text{(B-2)}$$

Figure 5 demonstrates the substitution of these torques into Euler's equations of motion.[35] Combined with various vector identities and simplifications in notation, these rotational equations are then rewritten

EULER'S EQUATIONS:

$$I_n \dot{\omega}_n + (I_{n+2} - I_{n+1})\omega_{n+2}\omega_{n+1} = 3(\mu/r^3)\, c_{3,n+2} c_{3,n+1} (I_{n+2} - I_{n+1}) + \rho \left[\underline{Q} \times \underline{\underline{B}}^T \underline{S}\right]_n$$

EQUIVALENCES:

$$c_{ij} = \underline{\Gamma}_i^T \underline{G}_j$$

$$\left[\underline{Q} \times \underline{B}^T \underline{S}\right]_n = q_{i+1}\, \underline{G}_{i+2}^T \underline{S}' - q_{i+2}\, \underline{G}_{i+1}^T \underline{S}'$$

$$\xi_n \triangleq (I_{n+2} - I_{n+1}) / I_n$$

$$\nu_{ij} = \rho q_i / I_j$$

STATE VARIABLE FORM:

$$\dot{\omega}_n = \xi_n (-\omega_{n+1}\, \omega_{n+2} + 3\mu\, \underline{\Gamma}_3^T \underline{G}_{n+2}\, \underline{\Gamma}_3^T \underline{G}_{n+1} / r^3) + \nu_{n+1,n}\, \underline{G}_{n+2}^T \underline{S}'$$

$$- \nu_{n+2,n}\, \underline{G}_{n+1}^T \underline{S}' \quad ; n = 1, 2, 3$$

Figure 5. Equations of Motion

(as suggested in Appendix A) in terms of the vehicle rates and known functions of the Euler angles. The specific relation between these angles and the vectors is given at the beginning of Appendix C.

APPENDIX C

EULER'S GEOMETRIC EQUATIONS

Figure 6 shows the transformation from vehicle axes to the temporary inertial coordinates which correspond to time t_{m-1}. In accordance with equation A-5, the sequence of rotations has the order (x, y, z); the expanded version of equation A-5 is

$$\underline{\underline{G}} = \begin{bmatrix} \cos X_3 \cos X_2 & \sin X_3 \cos X_1 + \cos X_3 \sin X_2 \sin X_1 & \sin X_3 \sin X_1 - \cos X_3 \sin X_2 \cos X_1 \\ -\sin X_3 \cos X_2 & \cos X_3 \cos X_1 - \sin X_3 \sin X_2 \sin X_1 & \cos X_3 \sin X_1 + \sin X_3 \sin X_2 \cos X_1 \\ \sin X_2 & -\cos X_2 \sin X_1 & \cos X_2 \cos X_1 \end{bmatrix} \quad \text{(C-1)}$$

The first expression for the angular rate vector $\underline{\omega}$ in figure 6 follows immediately from the diagram and the conventions adopted; from the diagram and equation C-1 it also follows that

$$\underline{j}_1 = \underline{j} \cos X_1 + \underline{k} \sin X_1 \quad \text{(C-2)}$$

and

$$\underline{k}_2 = \underline{k}_3 = \underline{i} \sin X_2 + \cos X_2 (-\underline{j} \sin X_1 + \underline{k} \cos X_1) \quad \text{(C-3)}$$

Collecting the coefficients of $\underline{i}$, $\underline{j}$, and $\underline{k}$,

$$\begin{bmatrix} X_4 \\ X_5 \\ X_6 \end{bmatrix} \underline{\underline{\Delta}} \begin{bmatrix} \omega_1 \\ \omega_2 \\ \omega_3 \end{bmatrix} = \begin{bmatrix} -\dot{X}_1 - \dot{X}_3 \sin X_2 \\ -\dot{X}_2 \cos X_1 + \dot{X}_3 \sin X_1 \cos X_2 \\ -\dot{X}_3 \cos X_1 \cos X_2 - \dot{X}_2 \sin X_1 \end{bmatrix} \quad \text{(C-4)}$$

and it can be verified by direct substitution that the position state variable derivatives are given by the expressions at the bottom of figure 6.

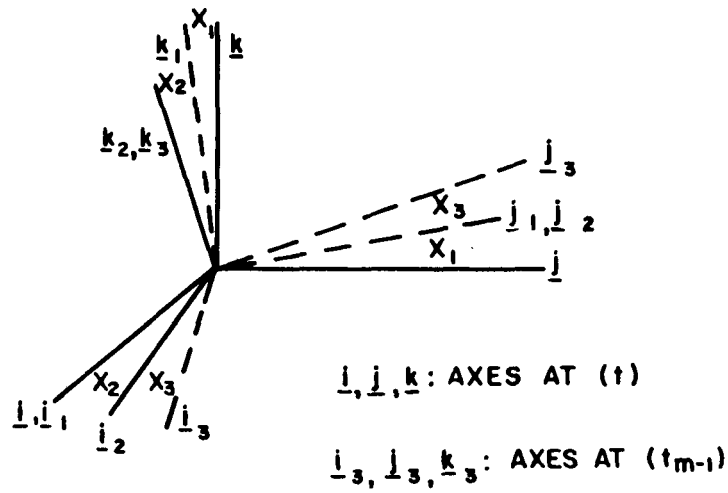

$$\underline{\omega} = -\dot{X}_1\ \underline{i} - \dot{X}_2\ \underline{j}_1 - \dot{X}_3\ \underline{k}_3 ;$$

$$\underline{\omega} = -\dot{X}_1\ \underline{i} - \dot{X}_2 (\underline{j}\ \text{COS}\ X_1 + \underline{k}\ \text{SIN}\ X_1) - \dot{X}_3 \left[\underline{i}\ \text{SIN}\ X_2 + \text{COS}\ X_2\ (-\underline{j}\ \text{SIN}\ X_1 + \underline{k}\ \text{COS}\ X_1)\right]$$

STATE VARIABLE FORM:

$$\dot{X}_1 = -X_4 + \text{TAN}\ X_2\ (X_6\ \text{COS}\ X_1 - X_5\ \text{SIN}\ X_1)$$

$$\dot{X}_2 = -X_5\ \text{COS}\ X_1 - X_6\ \text{SIN}\ X_1$$

$$\dot{X}_3 = -\text{SEC}\ X_2\ (X_6\ \text{COS}\ X_1 - X_5\ \text{SIN}\ X_1)$$

Figure 6. Euler's Geometric Equations

In these expressions the appearance of the tangent and secant of (X_2) clearly illustrates the singularity which would arise if (X_2) were allowed to approach a right angle.

APPENDIX D

RESTRICTIVE SOLUTION TO EULER'S EQUATIONS

For a torque-free satellite with dynamical symmetry about its x-axis (i.e., $I_2 = I_3 = I$), Euler's equations of motion reduce to

$$\dot{\omega}_1 = 0; \; I\dot{\omega}_2 = -(I_1 - I)\,\omega_1\,\omega_3; \; I\dot{\omega}_3 = (I_1 - I)\,\omega_1\,\omega_2 \qquad \text{(D-1)}$$

The solution to these equations can readily be expressed in terms of a spin rate (ω_A), a retrograde* precession rate (ω_B), the angle (α) between the spin axis ($\underline{i}$) and the angular momentum vector ($\underline{h}$); and a spin phase angle ($\omega_A t_A$). These constants are defined by the initial angular rate vector $\underline{\omega}_0$ as follows:

$$\omega_A = -\xi\,\omega_{01} \qquad \text{(D-2)}$$

$$\omega_B = I_1\,\omega_A \sec\alpha/(I_1 - I) = -(I_1/I)\,\omega_{01}\sec\alpha \qquad \text{(D-3)}$$

$$\alpha = \arctan\left\{I\omega_{yz}/I_1\,\omega_{01}\right\}, \quad 0 \le \alpha \le \pi \qquad \text{(D-4)}$$

$$\omega_A t_A = \arctan(\omega_{02}; \omega_{03}) \qquad \text{(D-5)}$$

where

$$\xi \triangleq (I_1 - I)/I \qquad \text{(D-6)}$$

$$\omega_{yz} \triangleq +\sqrt{\omega_{02}^2 + \omega_{03}^2} \qquad \text{(D-7)}$$

and the double argument inverse tangent of equation D-5 is defined as the inverse tangent of the ratio $(\omega_{02}/\omega_{03})$ with the quadrant dictated by

* The case $(I_1 > I)$, corresponding to spin stabilization about the major principal axis, is typical of most space applications.

the algebraic signs of the numerator and the denominator. In terms of these constants, the solution to equation D-1 may be written as

$$\omega_1 = \omega_{01} = -\omega_A/\xi \tag{D-8}$$

$$\omega_2 = -A_s\,\omega_A\,(\xi + 1)\tan\alpha/\xi \tag{D-9}$$

$$\omega_3 = -A_c\,\omega_A\,(\xi + 1)\tan\alpha/\xi \tag{D-10}$$

in which A_s and A_c are defined as the sine and cosine, respectively, of the composite angle $\omega_A\,(t + t_A)$. It is also noted that

$$\omega_2 = \omega_{02}\cos(\xi\omega_1 t) - \omega_{03}\sin(\xi\omega_1 t) \tag{D-11}$$

$$\omega_3 = \omega_{02}\sin(\xi\omega_1 t) + \omega_{03}\cos(\xi\omega_1 t) \tag{D-12}$$

This formulation corresponds to the XYX Euler angle sequence,

$$\underline{\underline{\eta}} \triangleq \left[\omega_B t\right]_x \left[-\alpha\right]_y \left[-\omega_A\,(t + t_A)\right]_x \tag{D-13}$$

and it can easily be verified that the derivative of this matrix is equal to the product,

$$\dot{\underline{\underline{\eta}}} = \begin{bmatrix} \alpha_c & \alpha_s A_s & \alpha_s A_c \\ -\alpha_s B_s & A_c B_c + \alpha_c A_s B_s & -A_s B_c + \alpha_c A_c B_s \\ -\alpha_s B_c & -A_c B_s + \alpha_c A_s B_c & A_s B_s + \alpha_c A_c B_c \end{bmatrix} \begin{bmatrix} 0 & \alpha_s\omega_B A_c & -\alpha_s\omega_B A_s \\ -\alpha_s\omega_B A_c & 0 & -\omega_A + \alpha_c\omega_B \\ \alpha_s\omega_B A_s & \omega_A - \alpha_c\omega_B & 0 \end{bmatrix} \tag{D-14}$$

where the subscripts (s, c) again denote the sine and cosine, respectively, of the angles contained in equation D-13. The correspondence between the off-diagonal terms of the above skew-symmetric matrix and the angular rates of equations D-8 to D-10 is easily established from the defining relationships given earlier. It follows that the premultiplying factor on the right of equation D-14 is a closed form solution for

vehicle attitude, complete to within a premultiplicative* constant matrix. Obviously, to satisfy the initial conditions, the complete transformation from vehicle to inertial coordinates must be

$$\underline{\underline{B}} = \underline{\underline{B}}_R \left[\omega_A t_A\right]_x \left[\alpha\right]_y \left[\omega_B t\right]_x \left[-\alpha\right]_y \left[-\omega_A (t + t_A)\right]_x \qquad \text{(D-15)}$$

where $\underline{\underline{B}}_R$ is the value of $\underline{\underline{B}}$ at the reference time.

The following comments will facilitate a rigorous interpretation of the preceding analysis:

1. The angular momentum vector in vehicle coordinates,

$$\underline{h} = \underline{i}\, I_1\, \omega_1 + I\,(\underline{j}\, \omega_2 + \underline{k}\, \omega_3) \qquad \text{(D-16)}$$

has a magnitude of $(I_1\, \omega_{01} \sec \alpha)$. The conventions adopted here ensure that, since (ω_{01}) and $(\sec \alpha)$ always have the same sign, this expression cannot of course be negative. It is easily verified that $(\underline{\underline{\eta}}\, \underline{h})$ has only an x - component.

2. The phase angle $\omega_A t_A$ is equal to the angle between $\underline{h}$ and the initial $\underline{k}$ axis. By including this in the transformation, it is ensured that the intermediate y-axis is indeed perpendicular to the plane of $\underline{h}$ and the initial vehicle x-axis. This paves the way for the middle transformation in (D-13).

3. By definition, the algebraic signs of (ω_{01}) and $(\cos \alpha)$ must agree. From (D-2) it follows that, when (ξ) is positive, (ω_A) is positive

---

* Postmultiplication of $\underline{\underline{\eta}}$ by a constant matrix would destroy the differential equation relationship for a transformation <u>from</u> vehicle <u>to</u> stabilized coordinates.

for obtuse (α) and negative for acute (α). From (D-3) it can be seen that ω_B always turns out negative with the conventions adopted here. * Since the spin and precession rates are of opposite sense in (D-13), it follows that positive values of (ξ) produce retrograde precession.

4. Force-free precession is described in various other references.[16, 36]

The solution given here for vehicle rates, attitude matrices, pertinent constants, and all angles, must be regarded as well known. It has been included here under a unified notation to provide a complete background for Appendix E.

* This could have been changed by redefining (α), restricting its value to acute angles, or by one of several alternate formulations. The matrix solution, however, would have to remain unchanged.

APPENDIX E

PRECESSION OF ANGULAR MOMENTUM BY SMALL TORQUES

For certain symmetrical spinning satellites under consideration in this study, a simplified formulation[26] of gravity gradient effects can be applied to the dynamic equations. In the absence of solar torque, satellite rotation is essentially described by a slight modification of the motion just defined (Appendix D). The angular momentum vector precesses about the orbit poie at an average rate of order (n_0^2). Immediately this suggests a straightforward extension of the analysis just performed, leading to modified expressions for the satellite attitude matrix. Such an extended analysis has been performed but, since it does not include the accompanying nutations, it has not been completely incorporated into the program.

When gravity gradient is absent (as is essentially true of solar orbiters or satellites at ten earth radii), satellite angular motion can be described by another modified formulation. The rotational dynamics in Appendix D can again be applied, with the angular momentum precessing about the sunline at a rate proportional to the solar torque.[27]

In the present simulation, closed form attitude matrix expressions are computed without the above precessional motions. This does not, of course, influence the results of the simulated attitude determination system performance; the closed form attitude matrices are used

merely to check the numerically integrated rotational dynamics. Evan these checks remain in very close agreement, due to the slow precession rates involved.

APPENDIX F

LIBRATION OF VERTICALLY ORIENTED SATELLITES

The immediate discussion will be limited to rigid satellites with no active or passive control torques and, for reasons which will be clear shortly, only circular orbits will be considered.

A nonspinning satellite can be locally stabilized by a gravity gradient torque which tends to align its yaw axis with the vertical* (see Appendix B). Stable motion of this type is characterized by an inertial angular velocity which is nearly equal to the orbital rate, having a direction which nearly coincides with the pitch axis. By linearizing Euler's equations for these conditions, approximate solutions describing the satellite angular motion can be obtained in closed form.[28] However, while this is valid for sufficiently small displacements from the reference orientation, the technique is subject to some unexpectedly severe restrictions.[29] In the case of three unequal principal moments of inertia, stability is unexpectedly sensitive, even for circular

* This is not the only stabilizing mode for gravity gradient torque, but it is of primary interest here.

orbits.* Since orbit ellipticity would further inhibit the stability, elliptical orbits are not treated analytically. In general, no effort is made to use linearization techniques except in conjunction with those conditions for which the stability restrictions are known.

For small angular displacements from reference local coordinates, the following approximations are introduced:

$$\underline{\underline{C}} \doteq \begin{bmatrix} 1 & \delta_3 & -\delta_2 \\ -\delta_3 & 1 & \delta_1 \\ \delta_2 & -\delta_1 & 1 \end{bmatrix} \tag{F-1}$$

$$\begin{bmatrix} \dot{\delta}_1 \\ \dot{\delta}_2 \\ \dot{\delta}_3 \end{bmatrix} \doteq \begin{bmatrix} -\omega_1 - \delta_3 n_0 \\ -\omega_2 + n_0 \\ -\omega_3 + \delta_1 n_0 \end{bmatrix} \tag{F-2}$$

Substituting these into Euler's equations of motion, retaining only first order terms,

$$I_1 \ddot{\delta}_1 + (I_3 + I_1 - I_2) n_0 \dot{\delta}_3 - 4 (I_3 - I_2) n_0^2 \delta_1 = 0 \tag{F-3}$$

* It is of interest to note that bounded (and therefore, stable) motion can be demonstrated by true nonlinear analysis in the symmetrical case.[37] In following the derivation given in reference 37, it is important to note that the energy integral is the Hamiltonian function, which is not equal to the total energy. This latter point is explained in an extended analysis along similar lines.[38]

$$I_2 \ddot{\delta}_2 + 3 (I_1 - I_3) n_0^2 \delta_2 = 0 \qquad \text{(F-4)}$$

$$I_3 \ddot{\delta}_3 - (I_3 + I_1 - I_2) n_0 \dot{\delta}_1 + (I_2 - I_1) n_0^2 \delta_3 = 0 \qquad \text{(F-5)}$$

These expressions are equivalent to equation I of reference 28, permuted and modified by appropriate notation changes. A restrictive closed form solution for small oscillations can be applied under the conditions summarized below:

1. Only earth satellites are considered.

2. No solar torque can be present.

3. The orbit must be circular.

4. Only small initial angular displacements are allowed; $(z_1^2 + z_2^2 + z_3^2)^{1/2} < 0.1$

5. For stability of vertical orientation, $I_1 > I_3$.

6. The stability conditions in reference 28 must be satisfied:*

$$\xi_1 \xi_3 < 0; \; F_1 = (1 - 3\xi_1 - \xi_1 \xi_3) > 0; \; F_2 = F_1^2 + 16 \, \xi_1 \xi_3 > 0 \qquad \text{(F-6)}$$

7. Only small initial values are allowed for the derivative $(\dot{\delta}_2)$:

$$\left| \omega_{02} - n_0 \right| \leq 0.1 \sqrt{3 \xi_2} \; n_0 \qquad \text{(F-7)}$$

and the initial rates $(\dot{\delta}_1, \dot{\delta}_3)$ must be negligible;**

$$\left| \omega_{01} + n_0 z_3 \right| < 0.01 \, (r_1 Z_{11} + r_2 Z_{21}) \qquad \text{(F-8)}$$

$$\left| \omega_{03} - n_0 z_1 \right| < 0.01 \, (r_1 Z_{13} + r_2 Z_{23}) \qquad \text{(F-9)}$$

---

* ξ's are defined in figure 5.

** This is not an essential restriction. It was adopted to simplify the analytical form without unduly limiting its scope.

where

$$r_1 = \frac{n_0}{\sqrt{2}} \sqrt{F_1 + \sqrt{F_2}}; \quad r_2 = \frac{n_0}{\sqrt{2}} \sqrt{F_1 - \sqrt{F_2}} \tag{F-10}$$

and

$$Z_{11} = \left[(R_{11} z_1)^2 + (R_{31} z_3)^2 \right]^{1/2}; \; Z_{21} = \left[(R_{21} z_1)^2 + (R_{41} z_3)^2 \right]^{1/2} \tag{F-11}$$

$$Z_{13} = \left[(R_{33} z_1)^2 + (R_{13} z_3)^2 \right]^{1/2}; \; Z_{23} = \left[(R_{43} z_1)^2 + (R_{23} z_3)^2 \right]^{1/2} \tag{F-12}$$

with the R-parameters defined as

$$\begin{bmatrix} R_{11} \\ R_{21} \\ R_{31} \\ R_{41} \end{bmatrix} = \frac{1}{r_1^2 - r_2^2} \begin{bmatrix} r_1^2 - n_0^2 (1 + \xi_1 - \xi_1 \xi_3) \\ r_2^2 - n_0^2 (1 + \xi_1 - \xi_1 \xi_3) \\ (1 + \xi_1) \xi_3 n_0^3 / r_1 \\ (1 + \xi_1) \xi_3 n_0^3 / r_2 \end{bmatrix} \tag{F-13}$$

$$\begin{bmatrix} R_{13} \\ R_{23} \\ R_{33} \\ R_{43} \end{bmatrix} = \frac{1}{r_1^2 - r_2^2} \begin{bmatrix} r_1^2 - n_0^2 (1 - \xi_3 - 3\xi_1 - \xi_1 \xi_3) \\ r_2^2 - n_0^2 (1 - \xi_3 - 3\xi_1 - \xi_1 \xi_3) \\ 4 (1 - \xi_3) \xi_1 n_0^3 / r_1 \\ 4 (1 - \xi_3) \xi_1 n_0^3 / r_2 \end{bmatrix} \tag{F-14}$$

8. All amplitudes (Z) are restricted to values below 0.1 radian. This limitation was chosen because of the plurality of unstable points in figures 8 and 9 of reference 29.

When the above eight conditions are satisfied, the angular displacement from the local reference can be closely approximated by uncoupled pitch oscillations,

$$\delta_2 = \left[z_2^2 + (\dot{\delta}_{02})^2 / 3\xi_2 n_0^2 \right]^{1/2} \cos\left\{ \sqrt{3\xi_2}\, n_0 t + \Psi_2 \right\} \tag{F-15}$$

and coupled yaw-roll oscillations,

$$\delta_1 = Z_{11} \cos (r_1 t + \Psi_{11}) - Z_{21} \cos (r_2 t + \Psi_{21}) \tag{F-16}$$

$$\delta_3 = Z_{13} \cos (r_1 t + \Psi_{13}) - Z_{23} \cos (r_2 t + \Psi_{23}) \tag{F-17}$$

where (see Appendix D for a definition of the double argument inverse tangent)

$$\Psi_2 = \arctan \left\{ -\dot{\delta}_{02};\ \sqrt{3\xi_2}\, n_0 z_2 \right\} \tag{F-18}$$

$$\Psi_{11} = \arctan \left\{ R_{31} z_3;\ R_{11} z_1 \right\} \tag{F-19}$$

$$\Psi_{21} = \arctan \left\{ R_{41} z_3;\ R_{21} z_1 \right\} \tag{F-20}$$

$$\Psi_{13} = \arctan \left\{ R_{33} z_1;\ R_{13} z_3 \right\} \tag{F-21}$$

$$\Psi_{23} = \arctan \left\{ R_{43} z_1;\ R_{23} z_3 \right\} \tag{F-22}$$

These closed form expressions are programmed as an independent check for the numerical integration of Euler's equations.

APPENDIX G

STATE VARIABLE EQUATIONS

The state variable forms of Euler's dynamic and geometric equations are given in figures 5 and 6, respectively. In addition to integrating these true equations of motion, the simulation determines the apparent state from the following relations:

$$\begin{bmatrix} \dot{\hat{X}}_1 \\ \dot{\hat{X}}_2 \\ \dot{\hat{X}}_3 \\ \dot{\hat{X}}_4 \\ \dot{\hat{X}}_5 \\ \dot{\hat{X}}_6 \end{bmatrix} = \begin{bmatrix} -\hat{X}_4 + \tan \hat{X}_2 \, (\hat{X}_6 \cos \hat{X}_1 - \hat{X}_5 \sin \hat{X}_1) \\ -\hat{X}_5 \cos \hat{X}_1 - \hat{X}_6 \sin \hat{X}_1 \\ -\sec \hat{X}_2 \, (\hat{X}_6 \cos \hat{X}_1 - \hat{X}_5 \sin \hat{X}_1) \\ \xi_1 \left[-\hat{X}_5 \hat{X}_6 + 3\mu \, (\hat{\underline{\Gamma}}_3)^T \hat{\underline{G}}_3 \, (\hat{\underline{\Gamma}}_3)^T \hat{\underline{G}}_2 / r^3 \right] + \nu_{21} \, (\hat{\underline{G}}_3)^T \hat{\underline{S}}' - \nu_{31} \, (\hat{\underline{G}}_2)^T \hat{\underline{S}}' \\ \xi_2 \left[-\hat{X}_6 \hat{X}_4 + 3\mu \, (\hat{\underline{\Gamma}}_3)^T \hat{\underline{G}}_1 \, (\hat{\underline{\Gamma}}_3)^T \hat{\underline{G}}_3 / r^3 \right] + \nu_{32} \, (\hat{\underline{G}}_1)^T \hat{\underline{S}}' - \nu_{12} \, (\hat{\underline{G}}_3)^T \hat{\underline{S}}' \\ \xi_3 \left[-\hat{X}_4 \hat{X}_5 + 3\mu \, (\hat{\underline{\Gamma}}_3)^T \hat{\underline{G}}_2 \, (\hat{\underline{\Gamma}}_3)^T \hat{\underline{G}}_1 / r^3 \right] + \nu_{13} \, (\hat{\underline{G}}_2)^T \hat{\underline{S}}' - \nu_{23} \, (\hat{\underline{G}}_1)^T \hat{\underline{S}}' \end{bmatrix} \tag{G-1}$$

where $\hat{X}_i$, $\dot{\hat{X}}_i$ denote the instantaneous observed state variable and its first time derivative, as determined by the simulated attitude tracking data processor; $\hat{\underline{G}}_i$ is the (ith) column of the orthogonal matrix,

$$\hat{\underline{\underline{G}}} = \begin{bmatrix} \hat{X}_3 \end{bmatrix}_z \begin{bmatrix} \hat{X}_2 \end{bmatrix}_y \begin{bmatrix} \hat{X}_1 \end{bmatrix}_x \tag{G-2}$$

$\hat{\underline{\Gamma}}_i$ is the (ith) column of the orthogonal matrix,

$$\underline{\underline{\Gamma}} = (\hat{\underline{\underline{C}}}_{m-1})^T \begin{bmatrix} 0 & 1 & 0 \\ 0 & 0 & 1 \\ 1 & 0 & 0 \end{bmatrix} \left[\theta_{m-1} - \theta \right]_z \begin{bmatrix} 0 & 0 & 1 \\ 1 & 0 & 0 \\ 0 & 1 & 0 \end{bmatrix} \tag{G-3}$$

and

$$\hat{\underline{S}}' = (\hat{\underline{\underline{B}}}_{m-1})^T \underline{S} \qquad \text{(G-4)}$$

Note that $\hat{\underline{\underline{\Gamma}}}$ and $\hat{\underline{S}}'$ both are independent time varying functions, since they involve only (1) the known observed attitudes in the past and (2) translational navigation and ephemeris data which can be assumed known from independent sources. It follows that equation G-1 represents the state variable relationship which can be used in the physical system to obtain the transition properties derived in Appendix H.

APPENDIX H

STATE TRANSITION MATRIX

The state variable equations are of the form,

$$d\underline{X}/dt = \dot{\underline{X}} (X_1, X_2, \cdots X_6, t) \tag{H-1}$$

Partial differentiation with respect to the state variables which correspond to time t_o can be written symbolically as

$$\partial\dot{\underline{X}}/\partial\underline{X}_0 = \left[\partial\dot{\underline{X}}/\partial\underline{X}\right]\left[\partial\underline{X}/\partial\underline{X}_0\right] \tag{H-2}$$

Interchanging the order of differentiation on the left side,

$$\dot{\underline{\underline{\Phi}}} = \underline{\underline{A}}\,\underline{\underline{\Phi}} \tag{H-3}$$

where

$$\underline{\underline{\Phi}} \triangleq \partial\underline{X}/\partial\underline{X}_0 \tag{H-4}$$

and

$$\underline{\underline{A}} \triangleq \partial\dot{\underline{X}}/\partial\underline{X} \tag{H-5}$$

The state transition matrix is the solution of equation (H-3) subject to the initial conditions,

$$\underline{\underline{\Phi}}(0) = \underline{\underline{I}}_{66} \tag{H-6}$$

Observed quantities are used throughout because the physical system will always use the updated estimate as the reference.

As a step in determining the A-matrix, it is convenient to write the last three state equations as

$$\dot{\hat{X}}_{i+3} = \xi_i \left[-\hat{\omega}_{i+1} \hat{\omega}_{i+2} + 3\mu (\hat{\underline{\Gamma}}_3)^T \hat{\underline{G}}_{i+2} (\hat{\underline{\Gamma}}_3)^T \hat{\underline{G}}_{i+1} / r^3 \right] + \nu_{i+1,1} (\hat{\underline{G}}_{i+2})^T \hat{\underline{S}}' - \nu_{i+2,1} (\hat{\underline{G}}_{i+1})^T \hat{\underline{S}}' ; \; i, j = 1, 2, 3 \quad \text{(H-7)}$$

from which it follows that

$$a_{i+3,j} = (3\mu \xi_i / r^3) (\hat{\underline{\Gamma}}_3)^T \left[\hat{\underline{G}}_{i+2} (\hat{\underline{\Gamma}}_3)^T \frac{\partial \hat{\underline{G}}_{i+1}}{\partial \hat{X}_j} + \frac{\partial \hat{\underline{G}}_{i+2}}{\partial \hat{X}_j} (\hat{\underline{\Gamma}}_3)^T \hat{\underline{G}}_{i+1} \right] \quad \text{(H-8)}$$

$$+ \left[\nu_{i+1,1} \left(\frac{\partial \hat{\underline{G}}_{i+2}}{\partial \hat{X}_j} \right)^T - \nu_{i+2,1} \left(\frac{\partial \hat{\underline{G}}_{i+1}}{\partial \hat{X}_j} \right)^T \right] \hat{\underline{S}}'$$

where the vectors $(\partial \underline{G}_n / \partial \hat{X}_j)$ follow from equation C-1;

$$\left[\partial \hat{\underline{\underline{G}}} / \partial \hat{X}_1 \right] = \left[\underline{0}_{31}, \; -\hat{\underline{G}}_3, \; \hat{\underline{G}}_2 \right] \quad \text{(H-9)}$$

$$\left[\partial \hat{\underline{\underline{G}}} / \partial \hat{X}_2 \right] = \left[\hat{\underline{G}}_3 \cos \hat{X}_1 - \hat{\underline{G}}_2 \sin \hat{X}_1, \; \hat{\underline{G}}_1 \sin X_1, \; -\hat{\underline{G}}_1 \cos \hat{X}_1 \right] \quad \text{(H-10)}$$

$$\left[\partial \hat{\underline{\underline{G}}} / \partial \hat{X}_3 \right] = \left[\hat{\underline{G}}_1 \times \underline{1}_3, \; \hat{\underline{G}}_2 \times \underline{1}_3, \; \hat{\underline{G}}_3 \times \underline{1}_3 \right] \quad \text{(H-11)}$$

In equation H-11, $\underline{1}_3$ is the column vector consisting of the components (0, 0, 1). Aside from this lower left submatrix, the other elements follow from inspection of the state equations. The complete matrix is

$$\underline{\underline{A}} = \begin{bmatrix} \dot{\hat{X}}_2 \tan \hat{X}_2 & -\dot{\hat{X}}_3 \sec \hat{X}_2 & 0 & -1 & -\tan \hat{X}_2 \sin \hat{X}_1 & \tan \hat{X}_2 \cos \hat{X}_1 \\ \dot{\hat{X}}_3 \cos \hat{X}_2 & 0 & 0 & 0 & -\cos \hat{X}_1 & -\sin \hat{X}_1 \\ -\dot{\hat{X}}_2 \sec \hat{X}_2 & \dot{\hat{X}}_3 \tan \hat{X}_2 & 0 & 0 & \sec \hat{X}_2 \sin \hat{X}_1 & -\sec \hat{X}_2 \cos \hat{X}_1 \\ a_{41} & a_{42} & a_{43} & 0 & -\xi_1 \hat{X}_6 & -\xi_1 \hat{X}_5 \\ a_{51} & a_{52} & a_{53} & -\xi_2 \hat{X}_6 & 0 & -\xi_2 \hat{X}_4 \\ a_{61} & a_{62} & a_{63} & -\xi_3 \hat{X}_5 & -\xi_3 \hat{X}_4 & 0 \end{bmatrix} \quad \text{(H-12)}$$

In the special case of zero torque and one axis of dynamic symmetry, the transition matrix can be obtained in closed form. The lower half is especially straightforward, following from inspection of equations

D-8, D-11, and D-12. The upper half is approached by generalizing equation A-5 to allow finite (nonzero) values of the initial Euler angles;

$$\left[X_3\right]_z \left[X_2\right]_y \left[X_1\right]_x = \left[X_{03}\right]_z \left[X_{02}\right]_y \left[X_{01}\right]_x \underline{\underline{G}} \qquad \text{(H-13)}$$

Defining the partial derivative matrices for $1 \leq j \leq 3$,

$$\left[\nabla_j X_1\right] = \begin{bmatrix} 0 & 0 & 0 \\ 0 & -X_{1s} & X_{1c} \\ 0 & -X_{1c} & -X_{1s} \end{bmatrix} \phi_{1j} \qquad \text{(H-14)}$$

$$\left[\nabla_j X_2\right] = \begin{bmatrix} -X_{2s} & 0 & -X_{2c} \\ 0 & 0 & 0 \\ X_{2c} & 0 & -X_{2s} \end{bmatrix} \phi_{2j} \qquad \text{(H-15)}$$

$$\left[\nabla_j X_3\right] = \begin{bmatrix} -X_{3s} & X_{3c} & 0 \\ -X_{3c} & -X_{3s} & 0 \\ 0 & 0 & 0 \end{bmatrix} \phi_{3j} \qquad \text{(H-16)}$$

with (s) and (c) denoting sine and cosine, respectively, equation H-13 can be differentiated thus:*

$$\begin{aligned} &\left[\nabla_j X_3\right]\left[X_2\right]_y\left[X_1\right]_x + \left[X_3\right]_z\left[\nabla_j X_2\right]\left[X_1\right]_x \\ &\qquad + \left[X_3\right]_z\left[X_2\right]_y\left[\nabla_j X_1\right] \\ &= \begin{bmatrix} 0 & \delta_{3j} & -\delta_{2j} \\ -\delta_{3j} & 0 & \delta_{1j} \\ \delta_{2j} & -\delta_{1j} & 0 \end{bmatrix} \underline{\underline{G}} \end{aligned} \qquad \text{(H-17)}$$

* Equation H-17 contains the special case conditions $X_{01} = X_{02} = X_{03} = 0$, substituted into the matrix equations after differentiation.

where (δ_{ij}) is the Kronecker delta function. This can be rewritten as

$$\begin{bmatrix} -g_{21} & -g_{22} & -g_{23} \\ g_{11} & g_{12} & g_{13} \\ 0 & 0 & 0 \end{bmatrix} \phi_{3j} + \begin{bmatrix} X_{1a}g_{12} - X_{1c}g_{13} & -X_{1a}g_{11} & X_{1c}g_{11} \\ X_{1a}g_{22} - X_{1c}g_{23} & -X_{1a}g_{21} & X_{1c}g_{21} \\ X_{1a}g_{32} - X_{1c}g_{33} & -X_{1a}g_{31} & X_{1c}g_{31} \end{bmatrix} \phi_{2j}$$

$$+ \begin{bmatrix} 0 & g_{13} & -g_{12} \\ 0 & g_{23} & -g_{22} \\ 0 & g_{33} & -g_{32} \end{bmatrix} \phi_{1j} = \begin{bmatrix} 0 & -\delta_{3j} & \delta_{2j} \\ \delta_{3j} & 0 & -\delta_{1j} \\ -\delta_{2j} & \delta_{1j} & 0 \end{bmatrix} \quad \underline{\underline{G}} \qquad \text{(H-18)}$$

It can easily be verified that this matrix relation is satisfied (under conditions of equations C-1 and H-6) by

$$\begin{bmatrix} \phi_{11} & \phi_{12} & \phi_{13} \\ \phi_{21} & \phi_{22} & \phi_{23} \\ \phi_{31} & \phi_{32} & \phi_{33} \end{bmatrix} = \begin{bmatrix} \cos X_3 \sec X_2 & -\sin X_3 \sec X_2 & 0 \\ \sin X_3 & \cos X_3 & 0 \\ -\cos X_3 \tan X_2 & \sin X_3 \tan X_2 & 1 \end{bmatrix} \qquad \text{(H-19)}$$

All that remains is the submatrix $(\partial X_i/\partial \omega_{0j})$ for $1 \leq i \leq 3$, which can be determined from a combination of equations C-1 and the identification of $\underline{\underline{G}}$ per Appendix D:

$$\underline{\underline{G}} = \left[\omega_A t_A\right]_x \left[a\right]_y \left[\omega_B t\right]_x \left[-a\right]_y \left[-\omega_A (t + t_A)\right]_x \qquad \text{(H-20)}$$

From the elements g_{11}, g_{21}, g_{31}, g_{32}, and g_{33} of equation C-1 it follows that

$$\partial X_1/\partial \omega_{0j} = -(g_{33} \nabla_j g_{32} - g_{32} \nabla_j g_{33}) \sec^2 X_2 \qquad \text{(H-21)}$$

$$\partial X_2/\partial \omega_{0j} = (\nabla_j g_{31}) \sec X_2 \qquad \text{(H-22)}$$

$$\partial X_3/\partial \omega_{0j} = -(g_{11} \nabla_j g_{21} - g_{21} \nabla_j g_{11}) \sec^2 X_2 \qquad \text{(H-23)}$$

where $\nabla_j(g_{mn}) \triangleq \partial g_{mn}/\partial \omega_{0j}$ with elements taken from equation H-20,

$$g_{11} = a_c^2 (1-B_c) + B_c \tag{H-24}$$

$$g_{21} = a_s a_c k_s (1-B_c) - a_s k_c B_s \tag{H-25}$$

$$g_{31} = a_s a_c k_c (1-B_c) + a_s k_s B_s \tag{H-26}$$

$$g_{32} = A_s (a_s^2 k_c + a_c^2 k_c B_c - a_c k_s B_s) - A_c (k_s B_c + a_c k_c B_s) \tag{H-27}$$

$$g_{33} = A_c (a_s^2 k_c + a_c^2 k_c B_c - a_c k_s B_s) + A_s (k_s B_c + a_c k_c B_s) \tag{H-28}$$

in which, finally, (k_s) and (k_c) are defined as the sine and cosine, respectively, of the phase angle $(\omega_A t_A)$ and the remaining subscripted quantities above are defined as in Appendix D.

It should be noted that, in the simulation, all transition matrix elements are computed from observed parameters. (The usual circumflex notation was omitted above, merely to facilitate the presentation.)

APPENDIX I

KALMAN FILTER EQUATIONS*

The minimum variance data processing equations are based upon a linearized representation of the transition from the state at the time of the last (m-1) measurement to the current (m) measurement time,

$$\underline{x}_m = \underline{\underline{\Phi}}_m \underline{x}_{m-1} \tag{I-1}$$

and the relations between observable and state are linearized thus:

$$y_m = \underline{H}_m \underline{x}_m \tag{I-2}$$

For a state uncertainty covariance $\underline{\underline{P}}$ and a measurement variance σ_m^2 it has been shown[17] that the minimum variance estimator can be computed recursively as

$$\underline{X}^{(+)} = \underline{X}^{(-)} + \underline{W}\,\hat{y} \tag{I-3}$$

where the superscripts (-) and (+) stand for immediately before and after the measurement, respectively, and

$$\underline{W} = \underline{\underline{P}}\,\underline{H}^T \left[\underline{H}\,\underline{\underline{P}}\,\underline{H}^T + \sigma_m^2\right]^{-1} \tag{I-4}$$

The current measurement produces a step reduction in uncertainty

$$\underline{\underline{P}}^{(+)} = \left[\underline{\underline{I}}_{66} - \underline{W}\,\underline{H}\right] \underline{\underline{P}}^{(-)} \tag{I-5}$$

---

* The expressions in this section are specialized to the case of independent scalar measurements.

and, between measurements, the uncertainty covariance matrix is extrapolated by the relation

$$\underline{\underline{P}}_m^{(-)} = \underline{\underline{\Phi}}_m \underline{\underline{P}}_{m-1}^{(+)} \underline{\underline{\Phi}}_m^T \tag{I-6}$$

Initial conditions for $\underline{\underline{P}}$ are provided by assuming a diagonal matrix with typical values of initial estimation error for angles and their rates. It has been shown that the diagonal matrix assumption is conservative.[39, 40]

APPENDIX J

SUNLINE MEASUREMENTS AND SENSITIVITIES

Figure 7 illustrates a sun sensor instrument face (normal to $\underline{L}_1$) with a slit (along the direction of $\underline{U}$) having a field of view such that, if

$$\underline{S}'' \cdot \underline{L}_1 > \cos 64 \text{ degrees} \tag{J-1}$$

then the angle (Y) will be directly measurable. The last expression of figure 7 can be written as

$$\cos Y = (\underline{S}')^T \underline{\underline{G}}\, \underline{L} / \left\{ 1 - \left[(\underline{S}')^T \underline{\underline{G}}\, \underline{U} \right]^2 \right\}^{1/2} \tag{J-2}$$

Denoting the angle between $\underline{S}''$ and $\underline{U}$ as (ζ), and taking variations in the observable and state,

$$-\sin Y\, \delta Y = (1/\sin^2 \zeta)\left\{ |\sin \zeta|\, (\underline{S}')^T \left[\sum_i (\partial \underline{\underline{G}}/\partial X_i)\, \delta X_i \right] \underline{L} \right.$$

$$\left. + (\underline{S}')^T \underline{\underline{G}}\, \underline{L} \, |\sin \zeta|^{-1} \cos \zeta\, (\underline{S}')^T \left[\sum_i (\partial \underline{\underline{G}}/\partial X_i)\, \delta X_i \right] \underline{U} \right\} \tag{J-3}$$

or

$$\delta Y = (-1/\sin^2 \zeta \sin Y)\, (\underline{S}')^T \left[\sum_i (\partial \underline{\underline{G}}/\partial X_i)\, \delta X_i \right] \underline{N} \tag{J-4}$$

where

$$\underline{N} \triangleq |\sin \zeta|\, \underline{L} + \cos Y \cos \zeta\, \underline{U} \tag{J-5}$$

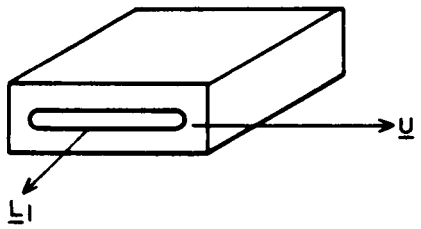

ADDITIONAL VECTORS

$$\underline{S}'' \triangleq \underline{\underline{B}}^T \underline{S} = \underline{\underline{G}}^T \underline{S}'$$

$$\underline{V} \triangleq \frac{\underline{S}'' \times \underline{U}}{|\underline{S}'' \times \underline{U}|} = \frac{\underline{S}' \times \underline{\underline{G}}\, \underline{U}}{|\underline{S}' \times \underline{\underline{G}}\, \underline{U}|}$$

MEASURED ANGLE = $Y = \arccos(\underline{V} \cdot \underline{L}_1)$;

$$Y = \arccos\left\{\frac{\underline{S}'' \cdot \underline{L}}{|\underline{S}'' \times \underline{U}|}\right\}, \quad \underline{L} \triangleq \underline{U} \times \underline{L}_1$$

$$Y = \arccos\left\{\frac{(\underline{S}')^T\, \underline{\underline{G}}\, \underline{L}}{|\underline{S}' \times \underline{\underline{G}}\, \underline{U}|}\right\}$$

Figure 7. Solar Measurements

It follows that, for i = 1, 2, 3,

$$\mathcal{H}_i = (-1/\sin^2 \zeta \sin Y)\, (\underline{S}')^T\, (\partial\, \underline{\underline{G}}/\partial X_i)\, \underline{N} \qquad \text{(J-6)}$$

and Y is of course insensitive to X_4, X_5, and X_6. The row vectors $(\underline{S}')^T\, \partial\, \underline{\underline{G}}/\partial\, X_i$ are determined from equations H-9 to H-11 using the conditions

$$(\underline{S}')^T\, \underline{G}_i = \underline{S}^T\, \underline{B}_i \qquad \text{(J-7)}$$

and

$$(\underline{1}_3)^T\, (\underline{S}') \times \underline{G}_i = (\underline{K}')^T\, \underline{S} \times \underline{B}_i \qquad \text{(J-8)}$$

in which each vector on the right was obtained by the transformation of its counterpart through the orthogonal matrix $\underline{\underline{B}}_{m-1}$. With these relations substituted into the appropriate equations,

$$(\underline{S}')^T \partial \underline{\underline{G}}/\partial X_1 = \left[0,\ -\underline{S}^T \underline{B}_3,\ \underline{S}^T \underline{B}_2\right] \tag{J-9}$$

$$(\underline{S}')^T \partial \underline{\underline{G}}/\partial X_2 = \left[\cos X_1\, \underline{S}^T \underline{B}_3 - \sin X_1\, \underline{S}^T \underline{B}_2,\ \sin X_1\, \underline{S}^T \underline{B}_1,\ -\cos X_1\, \underline{S}^T \underline{B}_1\right] \tag{J-10}$$

$$(\underline{S}')^T \partial \underline{\underline{G}}/\partial X_3 = \left[(\underline{K}')^T\, \underline{S} \times \underline{B}_1,\ (\underline{K}')^T\, \underline{S} \times \underline{B}_2,\ (\underline{K}')^T\, \underline{S} \times \underline{B}_3\right] \tag{J-11}$$

and

$$\mathcal{H}_1 = (-1/\sin^2 \zeta \sin Y)(-\underline{S}^T \underline{B}_3 n_2 + \underline{S}^T \underline{B}_2 n_3) \tag{J-12}$$

$$\mathcal{H}_2 = (-1/\sin^2 \zeta \sin Y)\left[(\cos X_1\, \underline{S}^T \underline{B}_3 - \sin X_1 \underline{S}^T \underline{B}_2)\, n_1 + \sin X_1\, \underline{S}^T \underline{B}_1\, n_2 - \cos X_1\, \underline{S}^T \underline{B}_1\, n_3\right] \tag{J-13}$$

$$\mathcal{H}_3 = (-1/\sin^2 \zeta \sin Y)\left[(\underline{K}' \cdot\ \underline{S} \times \underline{B}_1)\, n_1 + (\underline{K}' \cdot\ \underline{S} \times \underline{B}_2)\, n_2 + (\underline{K}' \cdot\ \underline{S} \times \underline{B}_3)\, n_3\right] \tag{J-14}$$

The preceding analysis was needed to determine accurate figures for measurement sensitivities. Instead of blindly applying these expressions in a complete simulation with an arbitrary measurement plan, however, it is highly desirable to further the investigation of

these coefficients for whatever insight they will afford at the outset. It has already been demonstrated[22] that the magnitude and the direction of ($\underline{\mathcal{H}}^T$) can be used to precondition the incoming data, allowing predictions in regard to (1) the usefulness of various measurements, (2) the approximate steady state error for a given observation accuracy, and (3) the regions where nonlinearity problems can be anticipated. For this purpose the analysis is continued, with approximations introduced wherever necessary, to provide a final expression of such simplicity that the measurement geometry vector can be closely characterized immediately upon inspection.

First, it is noted that, for nonspinning satellites, the angular displacement traversed between measurements will be small. Therefore, the Euler angles will be small. For spinning satellites, the first two Euler angles (X_1, X_2) will be small if the spin axis is chosen along the vehicle z-axis.* Therefore $\underline{K}' \doteq \underline{B}_3$, and

* This does not in any way restrict the allowable direction of the spin axis relative to the orbit; in the simulation, any space orientation of the vehicle z-axis can be selected through specification of the initial C-matrix. Use of the z-axis does fix the spin along a principal inertia axis, but this is not a severe restriction. It should be noted that this procedure tends to minimize pitch rates, thus avoiding singularity. Finally, when the x-axis is used instead of the z-axis, this analysis is still qualitatively correct, as explained later in this section.

$$\underline{K}' \cdot \underline{S} \times \underline{B}_1 \doteq - \underline{S}^T \underline{B}_2 \tag{J-15}$$

$$\underline{K}' \cdot \underline{S} \times \underline{B}_2 \doteq \underline{S}^T \underline{B}_1 \tag{J-16}$$

$$\underline{K}' \cdot \underline{S} \times \underline{B}_3 \doteq 0 \tag{J-17}$$

$$\sin X_1 \doteq 0; \cos X_1 \doteq 1 \tag{J-18}$$

and the approximate sensitivities are given by

$$\underline{\mathcal{H}}^T = (1/\sin^2 \zeta \sin Y) \underline{N} \times \underline{S}'' \tag{J-19}$$

It is immediately evident that the sun sensor provides information primarily concerning the angular displacement about an axis normal to the plane defined by the sunline and the instrument vector $\underline{N}$. Recognition of this fact will be useful for the initial selection of measurement plans and for anticipating troublesome geometric configurations.*

* Consider a spin-stabilized satellite with spin axis normal to the orbital plane which, in turn, is normal to the ecliptic. With 1 year, the situation will eventually arise in which all sun sensor measurements will be largely insensitive to the largest Euler angle of all.

As an aid in assessment of overall measurement sensitivity, the approximate magnitude of $\underline{\mathcal{H}}^T$ is

$$(1/\sin^2\zeta \sin Y)\left[(\underline{N}\times\underline{S}'')\cdot(\underline{N}\times\underline{S}'')\right]^{1/2} = \frac{\left[(\underline{N}\cdot\underline{N})(\underline{S}''\cdot\underline{S}'') - (\underline{N}\cdot\underline{S}'')^2\right]^{1/2}}{\sin^2\zeta \sin Y}$$

$$= \frac{\left\{\sin^2\zeta + \cos^2 Y \cos^2\zeta - \left[\left|\sin\zeta\right|\underline{L}\cdot\underline{S}'' + \cos Y \cos\zeta\, \underline{U}\cdot\underline{S}''\right]^2\right\}^{1/2}}{\sin^2\zeta \sin Y}$$

$$= \frac{\left[\sin^2\zeta + \cos^2 Y \cos^2\zeta - (\sin^2\zeta \cos Y + \cos^2\zeta \cos Y)^2\right]^{1/2}}{\sin^2\zeta \sin Y}$$

$$= \frac{1}{\left|\sin\zeta\right|}$$

This leads to two important implications in regard to desired measurement geometry:

1. For a given value of (ζ), the sensitivity is essentially independent of (Y). Since values of Y near 0 or 180 degrees are undesirable (because the plane of the angle and the algebraic sign of the deviation from nominal are ill defined) it follows that angles near 90 degrees form the best measurements.

2. Angles formed with low values of (ζ) can be used to some advantage, but excessively high sensitivities could cause nonlinearity.

It remains to demonstrate that these two conclusions are valid when the vehicle spins about its roll axis (as in formulations in earlier Appendices), instead of the yaw axis. Briefly, the entire small angle analysis holds for spin angles of $2K\pi$ ($K = 1, 2, 3, \ldots$); the sensitivities $\mathcal{H}_2$ and $\mathcal{H}_3$ are interchanged for spin angles of $(2K\pi + \pi/2)$; at intermediate spin angles a mere redistribution of sensitivity results.

APPENDIX K

MAGNETOMETER MEASUREMENTS AND SENSITIVITIES

A first approximation to the earth's magnetic field (which is adequate in this feasibility study) is a dipole with a magnetic moment $\underline{m}$, located at the earth center with a line of action at latitude 78.9°N and the earth longitude 70.1°W. The eastward celestial longitude at the equatorial intersection of the 70.1°W meridian is given in terms of an initial value ($\psi_{\beta 0}$) and the sidereal rate (ω_s) as illustrated in figure 8. This is used to determine the direction of $\underline{m}$ by the relation,

$$\underline{K}_\beta = \begin{bmatrix} k_{\beta 1} \\ k_{\beta 2} \\ k_{\beta 3} \end{bmatrix} = \begin{bmatrix} \cos 78.9° \cos \psi_\beta \\ \cos 78.9° \sin \psi_\beta \\ \sin 78.9° \end{bmatrix} \tag{K-1}$$

The flux density $\underline{\beta}$ given in figure 8 is easily reduced to [41]

$$\underline{\beta} = (-\mu_\beta \left| \underline{m} \right| / 4\pi) (\underline{K}_\beta \cdot \nabla) (\underline{R}/r^3) \tag{K-2}$$

which, in fixed inertial coordinates, has the components (n = 1, 2, 3):

$$\beta_n = (-\mu_\beta \left| \underline{m} \right| / 4\pi) \left[k_{\beta n}/r^3 - 3 (\underline{K}_\beta \cdot \underline{R}) r_n/r^5 \right] \tag{K-3}$$

The measured quantities are the components (β_n'') of the vector in body coordinates,

$$\underline{\beta}'' = \underline{\underline{B}}^T \underline{\beta} = \underline{\underline{G}}^T \underline{\underline{B}}^T_{m-1} \underline{\beta} = \underline{\underline{G}}^T \underline{\beta}' \tag{K-4}$$

$$\beta_\eta'' = \underline{G}_n^T \underline{\beta}' \tag{K-5}$$

CELESTIAL LONGITUDE OF MAG. POLE:

$$\psi_\beta = \psi_{\beta O} + \omega_S t$$

MAGNETIC POLE VECTOR:

$$\underline{K}_\beta \ (78.9°, \psi_\beta)$$

EARTH DIPOLE FIELD:

$$\underline{\beta} = \nabla \times \left\{-(\mu_O/4\pi)\left|\underline{m}\right| \underline{K}_\beta \times \nabla (1/r)\right\}$$

VEHICLE CO-ORDINATES:

$$\beta_n'' = \underline{B}_n^T \underline{\beta} = \underline{G}_n^T \underline{\beta}'$$

SENSITIVITY: $\partial \beta_n'' / \partial x_i = (\partial \underline{G}_n / \partial x_i)^T \underline{\beta}'$

APPROXIMATE SENSITIVITY: CROSS PRODUCT OF $\underline{\beta}$ WITH (n^{TH}) VEHICLE AXIS

Figure 8. Magnetic Field Measurements

the sensitivities are

$$\frac{\partial \beta_n''}{\partial X_i} = \left(\frac{\partial \underline{G}_n}{\partial X_i}\right)^T \underline{\beta}', \quad i = 1, 2, 3 \qquad \text{(K-6)}$$

where the vector partial derivatives ($\partial \underline{G}_n / \partial X_i$) are again taken directly from equations H-9 to H-11 and the vector $\underline{\beta}'$ is an independently known quantity.

Again using the small angle approximations in the partial derivatives ($\partial \underline{\underline{G}} / \partial X_i$) it is seen that

$$n = 1: \underline{\mathcal{H}} \doteq \left[0, \underline{G}_3{}^T \underline{\beta}', -\underline{G}_2{}^T \underline{\beta}'\right] = \left[0 \quad \beta_3'' \quad -\beta_2''\right] \tag{K-7}$$

$$n = 2: \underline{\mathcal{H}} \doteq \left[-\beta_3'' \quad 0 \quad \beta_1''\right] \tag{K-8}$$

$$n = 3: \underline{\mathcal{H}} \doteq \left[\beta_2'' \quad -\beta_1'' \quad 0\right] \tag{K-9}$$

Equation K-6 provides accurate values for measurement sensitivities, whereas equation K-7 to K-9 can be used for data conditioning criteria. Since $\underline{\mathcal{H}}_n{}^T$ is near the cross product of $\underline{\beta}$ with the nth vehicle axis, three considerations are immediately apparent:

1. A magnetometer with its sensitive axis instantaneously parallel to $\underline{\beta}$ will provide no attitude information.

2. The sensitivities experience their greatest changes at lower values of the angle between $\underline{\mathcal{H}}^T$ and $\underline{\beta}$. Readings of magnetometers in these positions should be avoided to prevent nonlinearity errors.

3. A magnetometer will be most effective when its sensitive axis is situated such that $\underline{\mathcal{H}}^T$ is close to the principal eigenvector of the attitude uncertainty covariance matrix.[21]

As in Appendix J, the use of a roll spin axis formulation will not invalidate the conclusions regarding data conditioning.

SELECTED BIBLIOGRAPHY

1. Macomber, G.R., and M. Fernandez, Inertial Guidance Engineering, London, Prentice-Hall, (1962).

2. Wiener, T.F., "Theoretical Analysis of Gimballess Inertial Reference Equipment Using Delta-Modulated Instruments," ScD Thesis T-300, Instrumentation Laboratory, Massachusetts Institute of Technology, Cambridge, Mass., (March 1962).

3. Bumstead, R.M. and W.E. VanderVelde, "Navigation and Guidance Systems Employing a Gimballess IMU," AIAA Guidance and Control Conference Paper No. 63-307, Massachusetts Institute of Technology, Cambridge, Mass., (August 12-14, 1963).

4. Powell, J.C., "The Present and Future Roles of Strapped-Down Inertial Systems," Transactions of the Eighth Symposium on Ballistic Missile and Space Technology, San Diego, Calif., Vol. 2, 162-178, (October 16-18, 1963).

5. Bessen, A.S. and J. Levine, "Strap-Down Navigation," Data Systems Engrg. 20, 6-11, (April 1965).

6. Quasius, G.R., "Strap-Down Inertial Guidance," Space Aeronautics 40, 89-94, (August 1963).

7. Blazek, H.F., "The Performance of Inertial Components on an Unstabilized Base," presented at ARS Controllable Satellites Conference, Massachusetts Institute of Technology, Cambridge, Mass., (April 30 - May 1, 1959).

8. Unger, F.G., "Vector and Matrix Representation of Inertial Instruments," Proceedings of IEEE Eleventh Annual ECCANE Conference, Baltimore, Md., 1.1.2-1 - 1.1.2-8 (October 21-23, 1964).

9. Sandeman, E.K., "FM Star-Lock System Using Mask With Linear Sectors," Trans. IRE ANE-9, 24-34 (1962).

10. Lowen, J.B. and M.S. Maxwell, "Scanning Celestial Attitude Determination System (SCADS)" Proceedings of IEEE Twelfth Annual ECCANE Conference, Baltimore, Md., 1.4.3-1 - 1.4.3-3 (October 27-29, 1965).

11. Hatcher, N.M. et.al., "Development and Testing of a Proposed Infrared Horizon Scanner for Use in Spacecraft Attitude Determination," NASA TN D-2995, (September 1965).

12. Black, H.D., "A Passive System for Determining the Attitude of a Satellite," AIAA J 2, 1350-1351 (1964).

13. Conley, J.M. and R.B. Patton Jr., "An Attitude Determining System for Spinning Rockets," Proceedings of IEEE Twelfth Annual ECCANE Conference, Baltimore, Md., 1.1.5-1 - 1.1.5-7 (October 27-29, 1965).

14. AD609-750, "Feasibility Study for a Vehicle Attitude Determining System; Vol. I - System Description and Analysis," Nov. 1964. (RADC Report No. RADC-TDR-64-318).

15. Wahba, G., "Problem 65-1, A Least Squares Estimate of Satellite Attitude," SIAM Rev. 7, 409 (1965).

16. Thomson, W.T., Introduction to Space Dynamics, New York, Wiley, p. 113-118, (1963).

17. Kalman, R.E., "A New Approach to Linear Filtering and Prediction Problems," J. Basic Eng. 82, 35-45 (1960).

18. Kalman, R.E. and R.S. Bucy, "New Results in Linear Filtering and Prediction Theory," J. Basic Eng. 83, 95-108 (1961).

19. Smith, G.L., S.F. Schmidt and L.A. McGee, "Application of Statistical Filter Theory to the Optimal Estimation of Position and Velocity on Board a Circumlunar Vehicle," NASA TR R-135, (1962).

20. McLean, J.D., S.F. Schmidt and L.A. McGee, "Optimal Filtering and Linear Prediction Applied to a Midcource Navigation System for the Circumlunar Mission," NASA TN D-1208, (1961).

21. Battin, R.H., "A Statistical Optimizing Navigation Procedure for Space Flight," ARSJ 32, 1681-1696 (1962).

22. Farrell, J., "Simulation of a Minimum Variance Orbital Navigation System," AIAA J. Spacecraft and Rockets 3, 91-98 (1966).

23. Danby, J.M.A., Fundamentals of Celestial Mechanics, New York, Macmillan, p. 7, (1962).

24. Ibid., pp. 155-156.

25. Stuelpnagel, J., "On The Parametrization of the Three-Dimensional Rotation Group," SIAM Rev. 6, 422-430 (1964).

26. Beletskii, V.V., "Motion of an Artificial Earth Satellite About Its Center of Mass," Artificial Earth Satellites, edited by L.V. Kurnosova (Plenum Press, Inc., New York, 1960) Vol. 1, pp. 30-59.

27. Clancy, T.F. and T.P. Mitchell, "Effects of Radiation Forces on the Attitude of an Artificial Earth Satellite," AIAA J 2, 517-524 (1964).

28. DeBra, D.B. and R.H. Delp, "Rigid Body Attitude Stability and Natural Frequencies in a Circular Orbit," J. Astronaut. Sci. 8, 14-17 (1961).

29. Kane, T.R., "Attitude Stability of Earth-Pointing Satellites," AIAA J 3, 726-731 (1965).

30. Tempelman, W.H., "Circular Orbit Partial Derivatives," AIAA J 1, 1187-1189 (1963).

31. Denham, W. and S. Pines, "Sequential Estimation When Measurement Function Nonlinearity is Comparable to Measurement Error," to appear in AIAA Journal.

32. Nidey, R.A., "Gravitational Torque on a Satellite of Arbitrary Shape," ARSJ 30, 203-204 (1960).

33. Roberson, R.E., "Gravitational Torque on a Satellite Vehicle," J. Franklin Inst. 265, 13-22 (1958).

34. Polyakhova, Ye.N., "Solar Radiation Pressure and the Motion of Earth Satellites," AIAA J 1, 2893 (1963).

35. Goldstein, H., Classical Mechanics, Addison-Wesley, Reading, Mass., p. 158, (1959).

36. Ibid., pp. 159-163.

37. Auelmann, R.R., "Regions of Libration for a Symmetrical Satellite," AIAA J 1, 1445-1447 (1963).

38. Pringle, R., "Bounds on the Librations of a Symmetrical Satellite," AIAA J 2, 908 (1964).

39. Schlegel, L.B., "Covariance Matrix Approximation," AIAA J 1, 2672-2673 (1963).

40. Hitzl, D.L., "Comments on 'Covariance Matrix Approximation'," AIAA J 3, 1977-1978 (1965).

41. Panofsky, W.K.H. and M. Phillips, Classical Electricity and Magnetism, Addison-Wesley, Reading, Mass., pp. 127-133, (1962).